

ELECTROACTIVITY OF ELECTROSPUN PVDF FIBER MATS AND
ZNO/PVDF COMPOSITES

by
ERDEM ÖĞÜT

Submitted to the Graduate School of Engineering and Natural Sciences
in partial fulfillment of
the requirements for the degree of
Master of Science

Sabanci University
August 2007

ELECTROACTIVITY OF ELECTROSPUN PVDF FIBER MATS AND
ZNO/PVDF COMPOSITES

APPROVED BY:

Assist. Prof. Dr. Melih Papila
(Thesis Supervisor)



Prof. Dr. Mehmet Akgün



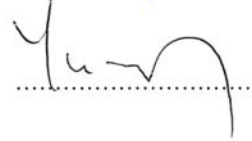
Assoc. Prof. Dr. Sedat Alkoy



Prof. Dr. Aydın Doğan



Assoc. Prof. Dr. Yusuf Ziya Menceloğlu



DATE OF APPROVAL: **13.08.2007**

© Erdem Ögüt 2007

All Rights Reserved

ELECTROACTIVITY OF PVDF ELECTROSPUN FIBER MATS AND ZNO/PVDF COMPOSITES

Erdem ÖĞÜT

Materials Science and Engineering, MSc Thesis, 2007

Thesis Supervisor: Assist. Prof. Dr. Melih PAPİLA

Keywords: PVDF, Electrospinning, Zinc Oxide, Piezoelectric Composite,
Electromechanical Characterization

Abstract

Poly(vinylidene fluoride) (PVDF), an electroactive polymer, has great distinctions for its mechanical properties compared to highly brittle electroceramics. Its piezoelectricity however is not immediately utilizable after being cast in film form, and the cast PVDF film requires additional processes, such as mechanical stretching and poling. In this thesis, alternative to cast PVDF film, electroactive characteristics of PVDF fibrous mats produced by electrospinning are investigated to seek whether it is sufficient to use them as piezoelectric actuator directly after their production.

The measurements revealed that under studied electrospinning parameter settings piezoelectricity of electrospun PVDF fibrous mat was not apparent, but the mat rather behaved as a linear dielectric. The transition from this linear to second order electric field dependence -that is interpreted as electrostrictive behaviour- is recorded.

Moreover, ZnO/PVDF electroactive composites, to combine features of ceramic and polymer materials, are produced by two methods. While ZnO is utilized as primary piezoelectric component, which does not require poling, PVDF is chosen as the matrix material to enhance the flexibility of the composite material. In the first process, a ZnO fibrous mat via electrospinning of precursor fibers and their calcination is dipped into a PVDF solution. In the second, ZnO and PVDF powders are mixed and casted as composite. Electroactive characterization showed that both processes result in a composite material with piezoelectric properties.

ELEKTRODOKUMA İLE ÜRETİLEN PVDF FİMLERİN VE ZNO/PVDF KOMPOZİTLERİN ELEKTROAKTİVİTESİ

Erdem ÖĞÜT

Malzeme Bilimi ve Mühendisliği, Yüksek Lisans Tezi, 2007

Tez Danışmanı: Yrd. Doç. Dr. Melih PAPİLA

Anahtar Kelimeler: PVDF, Elektrodokuma, Çinko Oksit, Piezoelektrik Kompozit,
Elektromekanik Karakterizasyon

Özet

Elektroaktif bir polimer olan Poli(viniliden florit) (PVDF), elektroseramik malzemelerin mekanik özellikleriyle karşılaştırıldığında önemli üstünlüklere sahiptir. Ancak, bu malzemenin -film olarak üretilir üretilmez- piezoelektrik özelliğinden yararlanılamamakta, mekanik esnetme ve kutuplama gibi ilave işlemlerin tatbikine ihtiyaç duyulmaktadır. Bu tezde, elektrodokuma yöntemiyle belirli üretim değişkenleri altında üretilen PVDF fiber ağ filmlerin -ek bir işleme tâbi tutulmaksızın- piezoelektrik eyleyici görevi görüp göremeyeceği, elektromekanik ölçümler vasıtasıyla incelenmiştir.

Ölçümler, mevcut üretim değişkenleri altında üretilen PVDF fiber ağ filmlerin piezoelektrik özelliğe sahip olmadığını, doğrusal dielektrik davranış gösterdiğini ortaya koymuştur. Fiber ağların elektroaktif özellikleri daha ayrıntılı olarak incelenmiş, elektrik alanla orantılı davranıştan -elektrostriktif olarak yorumlanan- elektrik alanın karesiyle orantılı davranışa geçiş cevapları gözlenmiştir.

Ek olarak, seramik ve polimer malzemelerin özelliklerini birleştirmek amacıyla, ZnO/PVDF kompozit malzemeleri iki ayrı yöntem ile elde edilmiştir. Kompozit malzemede ZnO, kutuplamaya ihtiyaç duymadan, piezoelektrik bileşen olarak kullanılırken, PVDF tutucu polimer olarak seçilmiştir. İlk işlemde, elektrodokuma ve sinterleme sonrası elde edilen ZnO fiber ağlarının kırılgenliği, PVDF çözeltisinin içine batırılıp çıkarılarak giderilmiş; ikincisinde, ZnO ve PVDF tozlarının karıştırılıp preslenmesi ile kompozitler üretilmiştir. Her iki işlemle de, piezoelektrik özelliğe sahip numuneler elde edilebildiği saptanmıştır.

Teyzeme...

ACKNOWLEDGEMENTS

I wish to express my sense of indebtedness to Dr. Melih PAPİLA -who is both my advisor and my thesis advisor- for his boundless guidance and advices during my study, and for the long discussions we have made together with him even during his intensive working hours. I am very lucky to have worked with him, from all directions.

I would like to thank to Dr. Yusuf MENCELOĞLU for his continuous help during my thesis and creative ideas he has given concerning my experimental work.

I am grateful to my thesis committee members Dr. Mehmet AKGÜN, Dr. Sedat ALKOY, Dr. Aydın DOĞAN, and Dr. Alpay TARALP for giving their valuable time commenting on my thesis.

I must express my thanks to Dr. Aydın DOĞAN for his help on the high-voltage experiments and Dr. Sedat ALKOY on the ferroelectric measurements.

I would also like to thank to Dr. Ayhan BOZKURT, Dr. Mehmet Ali GÜLGÜN, Dr. İsmet İnönü KAYA and Dr. Cleva OW-YANG for answering my questions and guiding on my experimental problems whenever I needed assistance.

My sincere thanks to Mehmet GÜLER and Bülent KÖROĞLU for helping me preparing the experimental setups.

I would like to express my gratitude to Dr. Melih PAPİLA's research team; Sinan, Mert, Bahar, Burçin, Ceren, Cihan and Özlem for their superior support and friendship; and my lab colleagues; Burak Abi, Cenk, Didem, Emre, Funda, İbrahim and Özge.

Finally, I would like to thank to my family for their boundless love and patience.

TABLE OF CONTENTS

Abstract.....	IV
Özet	V
1. INTRODUCTION	1
1.1 Objectives and Contribution.....	1
1.2 Review on Electrospun PVDF and ZnO Mats, and Electroactive Composites.....	2
1.2.1 Electrospun PVDF Mats	2
1.2.2 Electrospun ZnO Mats	5
1.2.3 Electroactive Composites	7
1.3 Ferroelectricity, Paraelectricity and Piezoelectricity:.....	9
1.3.1 Ferroelectricity.....	9
1.3.2 Paraelectricity	11
1.3.3 Piezoelectricity.....	14
1.3.4 Electrostriction.....	14
1.3.5 Poling.....	14
1.3.6 Hysteresis.....	15
2. MATERIALS PROCESSING	17
2.1 Electrospinning in Brief.....	17
2.2 Electrospinning of PVDF Fiber Mats	18
2.3 Electrospinning of ZnO Fiber Mats	19
2.4 ZnO / PVDF Electroactive Composites.....	21
2.4.1 ZnO Fibrous Mat/PVDF Fiber-Matrix Composite	22
2.4.2 ZnO Fibrous Mat/PVDF Fibrous Mat Composite	23
2.4.3 ZnO/PVDF Nanopowder Composite.....	23
3. ELECTROMECHANICAL CHARACTERIZATION	25
3.1 Measurement Setup.....	25
3.2 Coating and Sample Preparation.....	28
3.3 Determination of the Nature of Electroactivity	31

3.4	Faced Difficulties.....	35
4.	RESULTS AND DISCUSSIONS.....	37
4.1	PVDF Fibrous Mats.....	37
4.1.1	XRD.....	37
4.1.2	DSC.....	38
4.1.3	Electromechanical Characterization.....	39
4.1.3.1	Electrostriction in PVDF Fibrous Mats.....	39
4.1.3.2	Transition of Electrostrictive to Linear Dielectric Response.....	40
4.1.4	More Investigations on the Linear Dielectric Behaviour of PVDF Fiber Mats.....	47
4.1.5	Discussion on PVDF Fibrous Mats.....	48
4.1.6	Faced Difficulties.....	50
4.2	ZnO Fiber Mats.....	51
4.2.1	Effect of Zinc Acetate Solution concentration.....	51
4.2.2	Images by Scanning Electron Microscopy.....	52
4.2.3	X-Ray Diffractometry.....	53
4.3	ZnO / PVDF Electroactive Composites.....	54
4.3.1	ZnO Fibrous Mat/PVDF Fiber-Matrix Composite.....	54
4.3.2	ZnO / PVDF Nanopowder Composite.....	55
4.3.3	Electromechanical Characterization.....	55
5.	SUGGESTIONS FOR FUTURE WORK.....	57
6.	CONCLUDING REMARKS.....	59
7.	BIBLIOGRAPHY.....	60

LIST OF FIGURES

Figure 1 : Schematic representation of the orientation change of dipoles in a ferroelectric material. (a) Zero net electric polarization is present because the electric dipoles are randomly aligned; (b) a low field is applied. Some of the dipoles align themselves in the direction of the field, some do not; (c) a sufficiently high field is applied. A certain alignment in the dipoles eventuates; (d) although the field is removed, almost all of the dipoles preserve their pre-condition. The net electric polarization is lower than that of (c), however it exists. 11

Figure 2 : Representation of the paraelectric effect in a dielectric material by the distortion of the electron cloud from its nucleus. (a) Even in the absence of an external electric field, an electric field exists inside the dielectric; (b) an applied field distorts the electron cloud, and has the same direction with the polarization vector; (c) even if the field has switched sign it is again in the same direction with the polarization vector. 12

Figure 3 : Representation of paraelectric mechanism in a dielectric film pointing out that strain response is independent of orientation; (a) no electric field E is applied, so no net polarization P or strain ε exists; (b) an electric field through-the-thickness of the film is applied. P is in the same direction as E and ε points upwards; (c) the film is turned upside down and the same E is applied as in (b). ε again points upwards; there is no change in the direction of the strain vector even if the film is reoriented. 13

Figure 4 : Mechanical deformations of poled piezoelectric plates subjected to electric field. Arrows represent the poling direction. (a) Thickness and length; (b) radial; (c) thickness shear; and (d) bender (e.g. bimorph structures). Adapted from [47]. 15

Figure 5 : A typical hysteresis loop for electric field vs. polarization compared with a linear dielectric response. Adapted from [39]..... 16

Figure 6 : The electrospinning setup..... **Error! Bookmark not defined.**

Figure 7 : Schematic representation of sample preparation for calcination process..... 20

Figure 8 : Heating method for the calcination of polymer/acetate precursor fibers to produce ZnO fibers..... 20

Figure 9 : Process flow for fiber-based and powder-based production.....	22
Figure 10 : A part of ZnO fiber mat dipped into PVDF solution after acetone has evaporated.	23
Figure 11 : ZnO fiber mat sandwiched in between two PVDF fiber mats.	23
Figure 12 : ZnO/PVDF nanopowder composite pressed into a pellet.	24
Figure 13 : Schematic representation of the electroactivity measurement set-up	26
Figure 14 : Electromechanical measurement setup.	26
Figure 15 : Electromechanical measurement setup: A closer view to the fonic sensor probe together with the specimen.....	27
Figure 16 : A picture of a gold-electroded PVDF electrospun mat at the time of a measurement. Copper and aluminium films are adhered just below the sensor probe for the sake of reflectivity and noise-free signals.	27
Figure 17 : First electrode format: Electric field vector is through-the-thickness.....	29
Figure 18 : Gold-electroded PVDF electrospun mat used for through-the-thickness change measurements.....	29
Figure 19 : Second electrode format: Electric field vector is in-plane.	30
Figure 20 : Bent, tube-like specimen. The adhered reflective film created a sufficient working area for the fonic sensor probe.....	30
Figure 21 : Gold-electroded tubular PVDF electrospun mat specimen used for in-plane strain measurements.	30
Figure 22 : The target surface of the tubular specimen.	31
Figure 23 : Possibility #1: Piezoelectricity. Through-the-thickness configuration. (a) Directions of the electric field and intrinsic polarization vectors are the same; (b) as a result, the film expands.	33
Figure 24 : Possibility #2: Piezoelectricity. Through-the-thickness configuration. (a) The film is reversed, so the directions of the electric field and intrinsic polarization vector directions are in opposite; (b) as a result, the film shrinks.....	33
Figure 25 : Possibility #1: Dielectricity. Through-the-thickness configuration. (a) Directions of the electric field and induced polarization vectors are the same; (b) as a result, the film expands.	34
Figure 26 : Possibility #2: Dielectricity. Through-the-thickness configuration. (a) The film is reversed, however the directions of the electric field and induced polarization vector directions remain the same; (b) as a result, the film again expands.....	34

Figure 27 : Possibility #1: Piezoelectricity. Through-the-thickness configuration. (a) Directions of the electric field and intrinsic polarization vectors are the same; (b) as a result, the film expands.	34
Figure 28 : Possibility #2: Piezoelectricity. Through-the-thickness configuration. (a) The film is rotated 180° around the y-axis, so the directions of the electric field and intrinsic polarization vector directions are in opposite; (b) as a result, the film shrinks.....	34
Figure 29 : Possibility #1: Dielectricity. Through-the-thickness configuration. (a) Directions of the electric field and induced polarization vectors are the same; (b) as a result, the film expands.	35
Figure 30 : Possibility #2: Dielectricity. Through-the-thickness configuration. (a) The film is rotated 180° around the y-axis, however the directions of the electric field and induced polarization vector directions remain the same; (b) as a result, the film again expands.....	35
Figure 31 : Gold, copper and graphite coated samples exposed to electrode-pinning. ..	36
Figure 32 : XRD measurement results of PVDF electrospun mat.....	38
Figure 33 : Effect of electrical force on the fiber crystal structure.....	38
Figure 34 : DSC results of PVDF electrospun sample compared with a stretched PVDF solution cast sample.	39
Figure 35 : Electromechanical response of as-received electrospun PVDF fibrous mats (100µm thick) excited at 2000V, 1Hz. The displacement of the mats is approximately 0.042µm. a) The sign of the output remained always negative even if the input's sign changed; b) quadratic relation exists between the output and the input.....	40
Figure 36 : Driving voltage is 350V at 1.5Hz. Sample thickness is 100 µm. A maximum displacement of approximately 0.71µm resulted in the mats.....	41
Figure 37 : Driving voltage is 250V. A maximum displacement of approximately 0.39µm resulted in the mats.	41
Figure 38 : Driving voltage is 150V. A maximum displacement of approximately 0.17µm resulted in the mats.	41
Figure 39 : Driving voltage is 100V. A maximum displacement of approximately 0.09µm resulted in the mats.	42
Figure 40 : Driving voltage is 80V. A maximum displacement of approximately 0.06µm resulted in the mats.....	42
Figure 41 : Driving voltage is 50V. A maximum displacement of approximately 0.04µm resulted in the mats.....	42

Figure 42 : Driving voltage is 40V. A maximum displacement of approximately 0.03 μm resulted in the mats.....	43
Figure 43 : Scaled version of Figure 42. A maximum displacement of approximately 0.03 μm resulted in the mats.	43
Figure 44 : Driving voltage is 250V. A maximum displacement of approximately 0.6 μm resulted in the mats.....	43
Figure 45 : Driving voltage is 150V. A maximum displacement of approximately 0.21 μm resulted in the mats.	44
Figure 46 : Driving voltage is 100V. A maximum displacement of approximately 0.05 μm resulted in the mats.	44
Figure 47 : Driving voltage is 80V. A maximum displacement of approximately 0.01 μm resulted in the mats.....	44
Figure 48 : Driving voltage is 50V. A maximum displacement of approximately 0.05 μm resulted in the mats.....	45
Figure 49 : Driving voltage is 40V. A maximum displacement of approximately 0.04 μm resulted in the mats.....	45
Figure 50 : Driving voltage is 30V. A maximum displacement of approximately 0.02 μm resulted in the mats.....	45
Figure 51 : Driving voltage is 20V. A maximum displacement of approximately 0.01 μm resulted in the mats.....	46
Figure 52 : Driving voltage is 10V. A maximum displacement of approximately 0.009 μm resulted in the mats.	46
Figure 53 : Scaled version of Figure 52. A maximum displacement of approximately 0.009 μm resulted in the mats.	46
Figure 54 : Electric field (V/m) vs. Polarization (Q/m^2)	48
Figure 55 : Electrospun PVDF: E (V/m) vs. P_{max} (Q/m^2).....	48
Figure 56 : Commercial PVDF: E (V/m) vs. P_{max} (Q/m^2)	48
Figure 57 : LabView block diagram.....	51
Figure 58 : Zn is the precursor solution with the highest zinc content. As it is seen in these SEM images, excess amount of zinc precipitates over both the precursor fibers (a) and the ZnO fiber itself after calcination (b).....	52
Figure 59 : (a) Zinc is the precursor solution with the lowest zinc content. The precursor fibers are uniform and continuous. (b) ZnO particles cannot always form continuous fibers; they mostly break into pieces due to small amount of zinc content.....	52

Figure 60 : (a) Precursor fibers; (b) ZnO sample imaged by 200K magnified. Grains with an average diameter of 20nm can be easily seen on the fiber structure.	53
Figure 61 : XRD data obtained from ZnO samples. The peaks are similar to the characteristic peaks of the wurtzite structure.	54
Figure 62 : SEM image of ZnO mat dipped into PVDF solution.....	54
Figure 63 : A magnified image of Figure 62. Note on PVDF laying over and between the ZnO fibers.....	55
Figure 64 : SEM image of nanopowder-based composite.....	55
Figure 65 : Electromechanical response of PVDF/ZnO composite pellets: a) PVDF coated ZnO fibrous mat excited with 10V, 0.5Hz, b) PVDF coated ZnO fibrous mat laminated with PVDF excited with 50V, 1Hz, and c) PVDF and ZnO nanopowder-based composite excited with 50V, 1Hz sinusoidal.	56

LIST OF TABLES

Table 1 : Precursor solution and calcination parameters that were employed for the fabrication of ZnO fibers.....	19
---	----

LIST OF SYMBOLS AND ABBREVIATIONS

α -phase	Alpha phase
β -phase	Beta phase
Å	Angstrom
BaTiO ₃	Barium Titanium Oxide
CNT	Carbon Nanotube
SWCN	Single-Walled Carbon Nanotube
Cm	Centimeter
E _c	Coercive field
DAQ	Data Acquisition System
°C	Degree Celsius
K	Dielectric constant
DSC	Differential Scanning Calorimeter
DMF	Dimethylformamide
E	Electric field
eV	Electron volt
Gr	Gram
HYBAS	Hybrid Actuation System
Hz	Hertz
P _{ind}	Induced polarization
IR	Infrared Spectroscopy
P _{intr}	Intrinsic polarization
kHz	Kilohertz
kV	Kilovolt
PbTiO ₃	Lead Titanium Oxide
PZN-PT	Lead zinc niobate-lead titanate
PZT	Lead Zirconate Titanate

MAV	Micro Air Vehicle
μC	Micro coulomb
μl	Microliter
μm	Micrometer
mA	Milliampere
ml	Milliliter
mV	Millivolt
Min	Minute
MW	Molecular weight
MWCNT	Multiwall Carbon Nanotube
NFM	Nanofibrous membrane
Nm	Nanometer
N	Normal vector
X	Paraelectric susceptibility
Psi	Pound square inch
P	Polarization
PAPBA	Poly(aminophenylboronic acid)
PVA	Poly(vinyl alcohol)
PVDF	Poly(vinylidene fluoride)
PVDF-HFP	Poly(vinylidene fluoride-co-hexafluoropropylene)
PVDF-TrFE	Poly(vinylidene fluoride-trifluoroethylene)
RSM	Response Surface Methodology
V_{rms}	Root Mean Square Voltage
P_r	Remnant polarization
P_s	Saturation polarization
SEM	Scanning Electron Microscope
sec	Second
ε	Strain vector
TBAC	Tetrabutylammonium chloride
V	Volt
w/w	Weight by weight ratio
XRD	X-ray Diffraction
ZnO	Zinc Oxide

1. INTRODUCTION

1.1 Objectives and Contribution

The inspiration of this thesis emerges from the lack of high strain, low weight, flexible, chemically resistant and media-free electroactive actuators. There exists electronic ceramic materials providing high strains, but they are brittle and high in density (i.e. lead zirconium titanate (PZT)), and there exists electroactive polymers such as Ionic Polymer-Metal Composites, but they have certain limitations associated with their actuation media.

One of the two major objectives of this thesis is to process an electroactive polymer, Poly(vinylidene fluoride) (PVDF), by electrospinning at specific process parameters and characterize it in order to obtain flexible, low weight, chemically resistant and media-free electroactive PVDF fibrous mats. Considerable amount of effort is concentrated on the nature of electroactivity of the mats: whether they are to be used as a piezoelectric or an electrostrictive actuator. The second objective is to investigate whether using PVDF and ZnO both in their fibrous and powder form would produce electroactive ceramic/polymer composites while reducing the brittleness of ZnO via the presence of PVDF, acting as the matrix component.

The primary contribution of this thesis is as follows: Knowing in advance the electromechanical characteristics of electroactive films is crucial to decide whether to use them as actuators or sensors, as well as to decide on the design of the actuation/sensor mechanism. Forecasts made on the electroactive performance of *electrospun fibrous* PVDF films exist in literature, but to the author's knowledge, none of them have explicitly revealed and discussed their electric field-strain relationship and nature of electroactivity. This work aims to fulfill this necessity.

In the following chapters also transition of PVDF fibrous mats' electroactivity from first order to second order electric field dependence is presented. Certain characteristics such as frequency response and amplitude of this result may be useful for those who search for flexible, high voltage actuators.

The content of this thesis is organized as follows: In Chapter 1 a review on electrospun PVDF and ZnO mats, and electroactive composites is given. In addition, brief theoretical review concerning the electronic properties of engineering materials is presented. There; ferroelectricity, piezoelectricity and paraelectricity are defined and their relationship is discussed. In Chapter 2, the microstructural properties and the processing methods of the used materials is treated. Chapter 3 involves all about the electromechanical measurements where the method used to determine the nature of electroactivity of PVDF and ZnO films is of particular interest. Chapter 4 represents the XRD, DSC and electromechanical measurement results to seek a correlation among them. Chapter 5 makes discussions on certain results presented in Chapter 4. In Chapter 6, suggestions on reducing the workload of the experimental work are offered, as well as a roadmap on the immediate future work. Finally, in Chapter 7 the whole work is summarized by the help of a list of conclusions.

1.2 Review on Electrospun PVDF and ZnO Mats, and Electroactive Composites

The first two sections present a summary on the potential uses of electrospun PVDF and ZnO fibrous mats, and in some cases the electrospinning process itself. Secondly, a brief survey concerning electroactive composites is made.

1.2.1 Electrospun PVDF Mats

PVDF is appealing to numerous industries for its inexpensive, lightweight, biologically compatible and mechanically stable structure. It can undertake large amount of deformation while maintaining ample forces. It has expeditious response time, very low density, and eminent pliability when compared to electroactive ceramics and shape memory alloys. PVDF and its copolymers are widely applied materials in both actuation and sensing mechanisms, which can be stimulated thermally [1], optically [2] or electrically [3]. They can be utilized as fibers and films mostly in linear movement requirements in various engineering applications such as active micro air vehicle wings [4], piezo-laminated columns [5], and shape correction films in space applications [6]. Other applications may include: Proton exchange membranes [2], filtration membranes [7], structural health monitoring [8], endoscopic tactile sensors [9],

and macrofluidic control [10]. Kwon and Dzenis, for instance, embedded PVDF films of tens of microns thick into the graphite/epoxy (CFRP) composite laminates to monitor the tensile failure of unidirectional CFRP laminates [11].

By the electrospinning process, submicron-sized or micrometer-sized fibers can be produced both from synthetic and natural polymer solutions or melts. These fibrous forms have the potential to be utilized in a broad range of applications from lithium battery electrolytes to flexible actuators. Fibrous mats have almost the same mechanical and chemical properties with that of non-fibrous films. The most distinctive property of fibrous mats may be of having higher surface area and having a porous structure, which is utilized in many applications such as gas sensors and battery electrolytes.

As examples concerning biomedicine, Zhao et al. (2005) produced electrospun PVDF membranes of $\sim 45\mu\text{m}$ thickness with 50nm to 300nm fiber diameter for possible usage in biomedical scaffolds for tissue regeneration [12].

PVDF mats have also been studied to utilize them as biological sensors. For instance, to detect sensitively the existence of glucose in a flowing stream in the presence of other carbohydrates, and with negligible interference, reproducibility and storage stability Manesh et al. (2007) have electrospun PVDF with Poly(aminophenylboronic acid) (PAPBA) and have prepared a nanofibrous membrane (NFM) from the resulting composite to yield in a novel composite sensor electrode [13]. The PVDF/PAPBA-NFM composite has responded linearly to the detection of glucose within a certain molar range and with a response time of less than 6 sec. The high surface area of the electrospun mats and active sites available for sensing of glucose have been reported as the basis of this good-performance response.

Due to their nanoporous structure, PVDF electrospun fiber webs have a potential to be utilized as polymer electrolytes or separators for batteries. Because of this reason, Choi et al. (2004) have produced electrospun fibers with diameters ranging from 100nm to 800nm and have thermally treated them for a potential use [14]. Kim et al. (2004), similarly, has investigated the effect of varying polymer contents of the electrospinning solution on the electrolyte applications in lithium ion polymer batteries [15].

In the studies concerning the development of polymer electrolytes, so far, only inert, nonconductive fillers had been utilized. Lee et al. (2007) have been the first to investigate for the addition of multiwall carbon nanotubes (MWCNTs) on the morphology, thermal transition, and ionic conductivity of PVDF-HFP membranes [16]. By electrospinning, MWCNTs are uniformly distributed into PVDF-HFP matrix. To find out the effect of MWCNTs on the ionic conductivity of electrospun PVDF-HFP/MWCNT membranes, impedance measurements are carried out. MWCNTs have been detected improving the electrochemical performance over pristine PVDF-HFP membrane. As a result, it has been concluded that PVDF-HFP/MWCNT electrolyte membrane possesses good interfacial stability and has a potential to be utilized as electrolyte in lithium ion secondary battery.

In a recent study done by Yee et al. (2007) [17] tetrabutylammonium chloride (TBAC), a hygroscopic salt, has been introduced into the electrospinning solution and its effect on the crystalline phase variations of the resulting PVDF fibrous mats has been investigated. By adding 3 wt.% of TBAC and electrospinning this solution by a rotating disc collector, aligned fibers with a β -phase dominant crystal structure in which the c -axis of the crystallites having a preferred orientation along the fiber axis has been reported. The enhancement of the β -phase has been commented to be both due to TBAC and the electrospinning process itself. It has been stated that TBAC could have induced more *trans* conformers, and electrospinning -due to the Columbic forces acting on the rotating fibers on the disc collector- promoted inter-chain registration. In addition, due to the conductivity of the electrospinning solution, less bead formation has been observed during electrospinning. Concerning the future works of this thesis, as stated in the Chapter 6, the resulting films will be electromechanically characterized to see whether the enhancement of β -phase has made a change on the nature of electroactivity, since β -phase crystal structure has been known to be responsible for piezoelectric response.

Pawlowski et al. (2003) used electrospinning to create lightweight and electrically responsive wing-skins for micro air vehicle (MAV) wing frame designs [4]. They have optimized the individual ratios of the polymer+solvent mixture as the electrospinning solution and made preliminary actuation tests on the fiber-coated wing frames. The actuation was applied by AC voltage via attached leads on the wing. To obtain the largest strain response from the wing, the magnitude of the waveform was kept high (2kV peak-to-peak) and the frequency (6.7Hz) was calibrated to fit the resonant frequency of the wing. A perceptible

vibration was seen, but the strain characteristic was not analyzed, whether it was piezoelectric or not.

Another work on the electroactivity of PVDF mats has been done by Harrison et al. (2006) [18]. In that work they have proved the induction of electroactivity by the electrospinning process itself such that it provided induction of the polar β -phase and spontaneous orientation of the dipoles. Via XRD they show the increase in β -phase with increase in the high-voltage applied in the electrospinning process using three voltage levels: 10kV (0.44kV/cm), 15kV (0.66kV/cm) and 20kV (0.87kV/cm). In addition, by Infrared Spectroscopy (IR) they present the similarity between poled and electrospun PVDF films. They claim as a conclusion that they have eliminated for the direct contact or corona poling for the piezoelectric activity in electrospun PVDF fibrous mats. However, although certain techniques used in that study have shown logical results, the strain characteristics of these films have not been determined to result on the type of electroactivity present and to be able to directly show whether the produced films have permanent dipoles or not.

A broad study on the morphology, crystal structure and mechanical properties of PVDF fibrous mats has been accomplished by Yordem [19]. In that work, the effect of the type of the electrospinning solvent and the solvent mixture; the electrospinning voltage and the collector distance have been investigated to produce planar fibrous mats of uniform fibers. In addition, to predict the electrospun fiber diameter, an experiment-based process optimization technique, Response Surface Methodology (RSM), has been utilized with the applied voltage and collector distance as the design parameters. Apart from these, the effect of the electrospinning voltage on β -phase formation has been investigated by gradually increasing the process voltage and analyzing the β -phase peaks via XRD. It has been concluded β -phase enhancement may be due to the stretching of PVDF fibers (i.e. Columbic forces) during electrospinning.

1.2.2 Electrospun ZnO Mats

In recent years ZnO is of great interest due to its excess availability, being lead-free and piezoelectric¹, and its optical properties in concern with the photonics industry. In addition, it has been utilized in biomedical applications, since it is biologically safe and bio-compatible.

¹ ZnO's piezoelectric activity is due its non-centrosymmetric crystal symmetry, which does not require poling after being produced.

Because of these distinctive properties, ZnO has been utilized in microsystems and biotechnology [20].

There are various manufacturing techniques yielding with ZnO, and among all, electrospinning is the one that produces continuous and nano-scale fibers after certain calcination scheme [21-24]. Moreover, the effect of electrospinning parameters on the ZnO fiber geometry is well-known so that one has the possibility to produce fibers with desired properties. On its production, Yang et al. (2004) have introduced electrospinning of ZnO fibers and characterized them [25]. Wu and Pan have varied the calcination time of ZnO precursor and examined the change in fiber diameter as a result of it [24].

Viswanathamurthi et al. (2004) have investigated for the morphology and optical properties of ZnO fibers with diameters ranging from nanometer to micrometer, and have concluded that they have the potential to be used as light-emitting devices in nano-scale optoelectronic applications [26]. As in this thesis, ZnO fiber formation after electrospinning of PVA/zinc acetate solution has been obtained by high-temperature calcination in air. Under excitation at 325 nm the photoluminescence spectra presented an ultraviolet emission at 3.13 eV and a green emission at 2.21 eV. The advantage of electrospinning in the optical properties is that electrospinning creates fibers with higher surface area than in continuous thin films. It has been stated that this may provide high sensitivity and fast response time in optical properties.

Wu et al. (2007) have modified the electrospinning setup to produce highly-oriented ZnO fibers, from a PVA/zinc acetate precursor, with a length of several centimeters [27]. The fibers -different from the conventional process- have been collected between the tip of the voltage supply -consisting of sharp triangular metal sheet- and the collector. The difference lies in the fact that the fibers are collected between two electrodes, but not on a counter electrode. The success of producing centimeter-long nanofibers has been expressed to lie on i) the reduction of inter-electrode distance, ii) the use of a higher electric field six times higher than in conventional processes, iii) using an electrospinning solution with high concentration to let the solvent evaporate quickly.

A first report on in-situ fabrication of ZnO nanocrystals with 1D polymer nanoarchitectures has been done by Hong et al. (2006) [28]. Two different routes has been

followed: In the first, to obtain PVA nanofibers with ZnO crystals residing on their surface, PVA/distilled water/zinc acetate/acetic acid solution has been electrospun and the resulting mat has been immersed in an ethanol solution. As a consequence of this immersion, ZnO precursors have been hydrolyzed to result with ZnO crystals residing on the fiber surfaces: a hybrid fiber. The reason for this behaviour has been concluded likely due to the inter-diffusion of molecules in polymer fiber matrix during hydrolysis. In the second route, ZnO-encapsulated PVA nanofibers were produced. This was done by preparing an aqueous colloidal nanocrystal ZnO solution, adding with PVA and electrospinning it. As a result, formation of ZnO nanocrystals residing within the PVA fibers has been accomplished. The produced membranes are expressed to be used as optical, antibacterial, and gas sensor membranes.

1.2.3 Electroactive Composites

There are mainly two reasons for producing electroactive composites. The first one concerns with developing structurally stable (mechanically, chemically etc.) materials by choosing the constituents having complementary properties. For example, one may want to improve on the structural properties of an electroactive material, which may be brittle and chemically weak, by treating the active part as the filler component and the inactive part as the matrix component having mechanically and chemically stronger properties. The second reason is to build actuators. Since actuators are generally desired to bend to generate out-of-plane strains, the active part is integrated with other active or inactive parts yielding in unimorph or bimorph actuators [3]. Various types of constituents may be used in the fabrication of composite materials. Micro or nano-constituents are usually fillers such as nanoparticles, chopped or continuous fibers/rods/tubes such as carbon nanotubes and ceramic rods. Matrix constituents, on the other hand, are bulk materials.

For instance, in the study of Cui et al. (1996) [29] they have embedded piezoelectric ceramic particles in a polymer matrix to get a 0-3 phase connectivity pattern, a high figure of merit, a low dielectric loss, pressure independent performance and thermal stability. As an additional note, they have emphasized on using low dielectric constant ceramic components in a composite material to be able to pole the material with increased efficiency. Noteworthy to say that dispersion quality of the nanoparticles is one of the important effects in fulfilling the final design goal. As in the above study, dispersion may be employed with a pre-determined connectivity pattern that's variation affects spatial properties of the composite.

Lee et al. (2003) used pairs of PVDF layers with electrically insulated interface layer for one point collocated sensor/actuator application on beam motion control [30]. Kim et al. (2005) reported a laminated structure composed of fiber reinforced plastic (FRP) laminate and piezoelectric ceramic wafer layer, lightweight piezo-composite actuator (LIPCA) [31]. The FRP was incorporated in order to provide the durability and protection to brittle PZT layer which is the electroactive ingredient. They investigated the effect of lay-up and demonstrated LIPCA can generate larger actuating displacements compared to traditional unimorph actuators.

In-situ health monitoring of structural systems such as ultrasonic transducers or acoustic emission sensors [11, 32-36] are also utilized from electroactive composites. In conventional health monitoring systems, the active polymeric layer is not embedded into the system, but it is integrated to it as an external structure. However in in-situ systems the active layer is embedded, so that the system works as a whole. As an example, Kwon and Dzenis have monitored the tensile failure of unidirectional graphite/epoxy laminates by embedding PVDF films into it as piezoelectric sensors [11].

Su et al. (2004) have developed a hybrid actuation system (HYBAS) using an electrostrictive polymer (PVDF-TrFE) and an electrostrictive ceramic single crystal (PZN-PT), which derives larger strain, hence a better efficiency, due to the individual contribution of the elements [37]. They have both theoretically modeled the strain response of the system and actuated it in a real environment. 220 μ m displacement at 800V_{rms} has been obtained. The developed polymer-ceramic hybrid system has been reported to derive larger strain, hence a better efficiency, due to the individual contribution of the elements. On the other hand, it has been stated that the polymer part could not adhere to the ceramic part, thus one could not provide a cooperative -mutual- property from the hybrid structure.

Concerning the production in this thesis, constituents have been utilized for the reason that -the ceramic- ZnO be as-produced piezoelectric but brittle, and PVDF requiring poling for piezoelectricity but being flexible. Although there are studies on enhancing the mechanical properties of ceramic materials [38], they are generally fragile under plying. Hence, the composition of a polymer matrix and a ceramic fiber is likely to alleviate assets regarding both mechanical and piezoelectric responses. As examples, Stroyan [39] has processed and characterized PVDF/PZT composite films and demonstrated 7.5 times increase in the peak

polarization compared to plain PVDF. Su et al. have developed PVP/ZnO composite fibers, but did not investigate the fibers for piezoelectricity [37]. Kowbel et al. (1998) have developed and characterized integrated actuator/sensor thin polymer based composites. Their investigation covered several piezo-composites. Low-porosity PZT infiltrated with Ceraset polymer composites have yielded enhancement in sensor while diminishing the actuator properties [40]. Flexible piezo-composites about 0.5 mm thick by powder mixing (PZT/PVDF) and subsequent pressing have easily been manufactured and resulted in significantly enhanced sensor properties. Films have offered improved actuation capability compared to plain PVDF, and improved sensor capability compared to PZT.

By electrospinning PVDF/DMF solution together with conductive carbon nanotubes (CNTs), Seoul et al. (2003) have aimed to produce conductive polymer/CNT fibrous composite mats via controlling the viscosity and the surface tension of the electrospinning solution [41]. In that work, they have examined the effect of the content of single-walled carbon nanotubes (SWCN) on the resulting fibrous mats as a goal to optimize the percolation threshold. In addition, they have made electrical conductivity measurements -by a Keithley 617 Electrometer- using the two-probe method on CN/PVDF/DMF solutions, CN/PVDF spin-coated films, and CN/PVDF electrospun fibrous mats. The thinnest composite film they have produced was 70nm.

1.3 Ferroelectricity, Paraelectricity and Piezoelectricity:

1.3.1 Ferroelectricity

The below two definitions state the musts of a ferroelectric material:

1. *“The defining characteristic of a ferroelectric is that the direction of polarization is switchable; it can be changed in direction (with a limited set determined by the crystal symmetry) through the application of a sufficiently high electric field.”* [42]
2. *“Ferroelectric materials retain their polarization even after an external field is removed.”* [43].

So, a ferroelectric material has symmetries that allow it to remain polarized in the absence of electric field, where the polarization direction can be reoriented by the application of a sufficiently high electric field. Ferroelectric materials are mostly based on the titania compounds with perovskite structure, such as BaTiO₃ and PbTiO₃. On the other hand, PVDF, a semi-crystalline polymer, which is of prime interest in this thesis, is also known as a ferroelectric.

Generally speaking, ferroelectric crystals own:

1. Electric dipoles (acquired from to the first definition).
2. Permanency of these dipoles (acquired from to the second definition)

Other explanatory notes on ferroelectricity can be listed as follows:

- The unit cells of a ferroelectric *may* arrange themselves in such a way that the whole material containing them would exhibit a net electric polarization. If it *may* not, each unit cell will own a randomly-directed electric dipole relative to the others, which in the whole will create a net zero electric polarization. This is depicted in Figure 1a. In addition, Figure 1 as a whole expresses the alignment process, which yields a net electric polarization by the application of a sufficiently high electric field.
- Ferroelectric crystals are polar, but being polar does not necessitate being ferroelectric: *Even if a material is polar, if the polarization is not reversible with the field the crystal is not named as a ferroelectric.*
- Ferroelectric crystals are pyroelectric and piezoelectric, but piezoelectric or pyroelectric crystals are not necessarily ferroelectric.

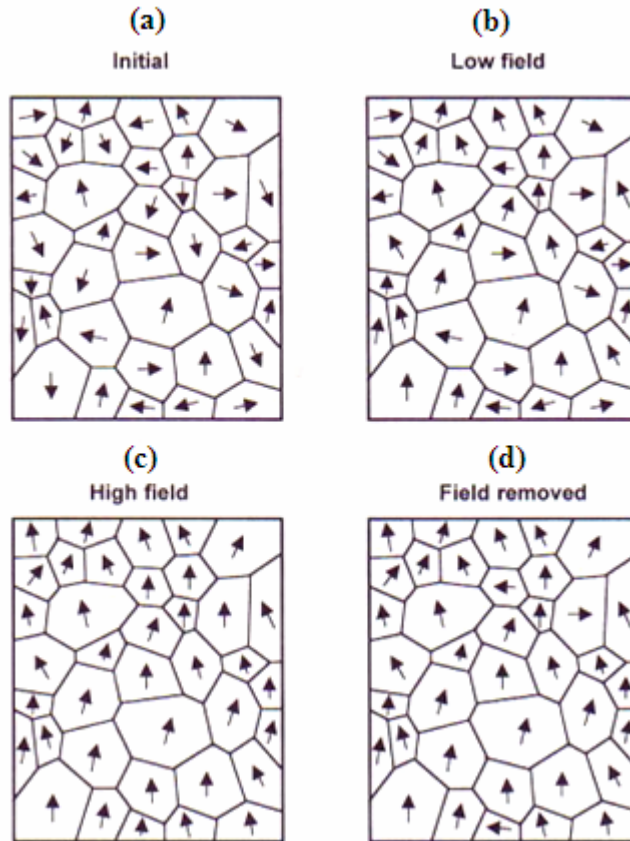


Figure 1 : Schematic representation of the orientation change of dipoles in a ferroelectric material. (a) Zero net electric polarization is present because the electric dipoles are randomly aligned; (b) a low field is applied. Some of the dipoles align themselves in the direction of the field, some do not; (c) a sufficiently high field is applied. A certain alignment in the dipoles eventuates; (d) although the field is removed, almost all of the dipoles preserve their pre-condition. The net electric polarization is lower than that of (c), however it exists.

1.3.2 Paraelectricity

As seen in Figure 2a, even in the absence of an external electric field, an electric field exists inside a dielectric (insulator) because of the attraction between the negatively charged electron cloud and the positively charged nucleus in each atom. Thus, electric field vectors are directed from positive to negative. In addition, because no electrical force is exerted on the electrons they are symmetrically distributed about the nucleus; so, the center of the negative charges coincides with the position of the nucleus. Because of this coincidence, the field vectors sitting in opposite directions around the nucleus cancel each other giving zero net electric dipole moment per unit volume, in other words, a zero net polarization (P).

We see in Figure 2b and Figure 2c that an applied electric field causes a distortion of the circular shaped electron cloud by pushing the electrons in one direction and the nucleus in the opposite direction. As a result, the center of the atom's negative charge no longer coincides

with the position of the nucleus, consequently, electric field vectors are no longer equal in magnitude and do not cancel each other because of the varying distance between the electrons and the nucleus.² This gives a net electric dipole moment per unit volume or net polarization different from zero. *The magnitude of the distance between the positive and negative charges' centers as well as their alignment direction is determined by the electric field (for low values) and does not depend on the orientation of the material.* The formed dipoles are thus called *temporary* electric dipoles and this behaviour is owned by paraelectric materials. So, the mechanism of paraelectric behaviour is defined as:

“The mechanism giving rise to paraelectric behaviour is the distortion of ions (displacement of the electron cloud from the nucleus) and the polarization of molecules or combinations of ions or defects.” [42].

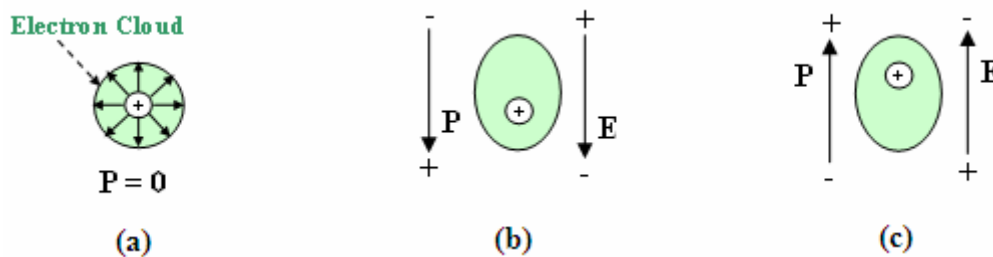


Figure 2 : Representation of the paraelectric effect in a dielectric material by the distortion of the electron cloud from its nucleus. (a) Even in the absence of an external electric field, an electric field exists inside the dielectric; (b) an applied field distorts the electron cloud, and has the same direction with the polarization vector; (c) even if the field has switched sign it is again in the same direction with the polarization vector.

In Figure 3 this mechanism is depicted on a dielectric film to point out that the strain behaviour is independent of film orientation. In piezoelectrics however, it changes when the film is reoriented. During the measurements this fact is used to conclude on nature of electroactivity, which is explained in 3.3.

² For simplicity, it is assumed that the electric field felt by the atom is the same as the overall electric field applied to the dielectric.

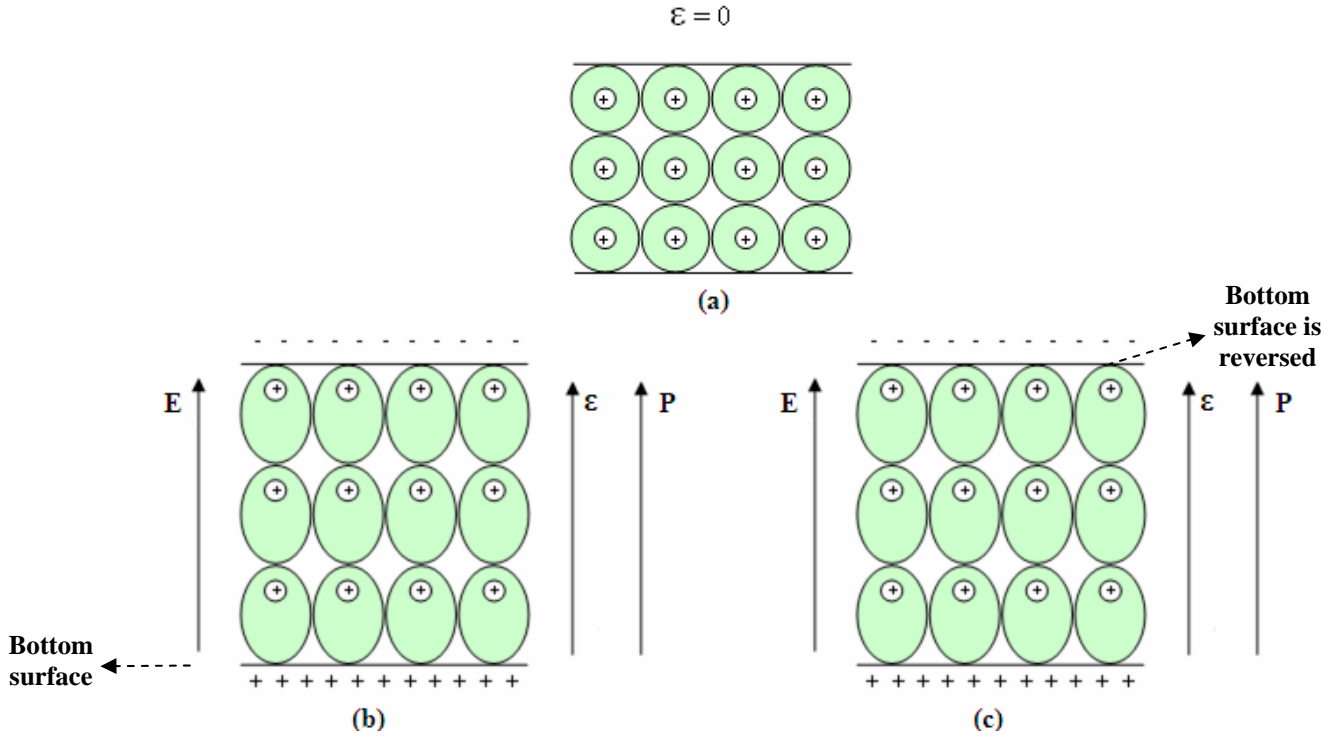


Figure 3 : Representation of paraelectric mechanism in a dielectric film pointing out that strain response is independent of orientation; (a) no electric field E is applied, so no net polarization P or strain ϵ exists; (b) an electric field through-the-thickness of the film is applied. P is in the same direction as E and ϵ points upwards; (c) the film is turned upside down and the same E is applied as in (b). ϵ again points upwards; there is no change in the direction of the strain vector even if the film is reoriented.

To summarize:

- A material is paraelectric if temporary polarization (P , in $\mu\text{C}/\text{cm}^2$) can be induced by an applied field (E , in kV/cm) even if no permanent electric dipoles exist in it.
- As a consequence, if the field is removed, the material returns to its initial state, i.e. zero polarization.
- In a paraelectric material, the applied field and polarization are linearly proportional, that is, polarization increases linearly with electric field, up to a certain field range. The proportionality between E and P is dielectric susceptibility:

$$\chi = \frac{P}{E\epsilon_0} \quad (2.1)$$

The dielectric constant κ and the susceptibility are related by: $\kappa = 1 + \chi$.

1.3.3 Piezoelectricity

The word “piezoelectricity” connotes to electric charge (i.e. electricity) induced by pressure (i.e. piezo³). This corresponds to the direct piezoelectric effect, in which charges develop due to an applied stress (or strain) on the material’s surface. The indirect effect, on the other hand, is in which mechanical stress (or strain) develops due to an applied electric field.

Like paraelectricity, piezoelectricity has a linear relationship between an applied stress and the resulting charge; however unlike paraelectrics, a material requires net non-zero polarization to be named as a piezoelectric. In addition, piezoelectrics have the ability to generate mechanical strain (or stress) when an electric field (or electric charge) is applied. This is called the indirect piezoelectric effect.

From an engineering point of view, direct piezoelectricity is utilized in sensor applications to “sense” a stimulus coming from the environment via the amount charge accumulating on its surface, whereas inverse piezoelectricity is utilized in actuation mechanisms, to apply stress or strain according to the potential difference applied on it.

1.3.4 Electrostriction

As mentioned in 1.3.3 when an electric field is applied to a piezoelectric or ferroelectric material, its dimensions change. On the other hand, once the field value is sufficiently increased a quadratic relationship supersedes the linear relationship between field and strain. This is the electrostrictive response.

1.3.5 Poling

Until the 1950s it is believed that only single-crystal materials exhibited piezoelectricity. There are however many ferroelectric materials that have randomly aligned dipoles, which can be added up by a certain process to yield a net electric polarization. This process is called poling, which is the application of a sufficiently high electric field to polarize the substance. This is depicted in Figure 1. There are several poling methods both for ceramics and polymers such as corona poling [44-46] and vacuum poling.

³ In Greek the word “piezo” means to “press”.

Prior to actuating a poled ferroelectric material it is essential to know both the direction of polarity and electric field to determine the direction of motion of the material. When applied field direction (positive to negative) is the same as the poling direction expansion will occur. However when they are opposite shrinkage will develop. This is schematically represented by Buchanan in Figure 4 where the arrows on the films and disks represent the poling direction.

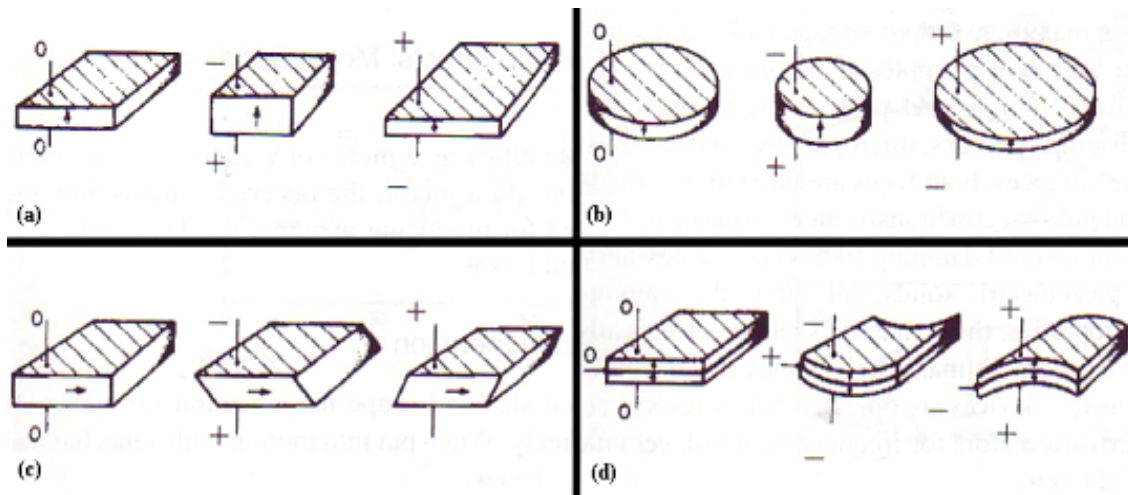


Figure 4 : Mechanical deformations of poled piezoelectric plates subjected to electric field. Arrows represent the poling direction. (a) Thickness and length; (b) radial; (c) thickness shear; and (d) bender (e.g. bimorph structures). Adapted from [47].

1.3.6 Hysteresis

Resistance to domain switching in a ferroelectric causes the polarization response to be nonlinear (i.e. hysteretic) rather than linear. The hysteretic polarization is switchable, that is, it changes sign with the electric field; however it is not completely reversible: Note in Figure 5 that even if the electric field is zeroed, there remains a certain amount of polarization.

Let one start to apply an electric field to a material that has zero macroscopic polarization, however which possesses electric dipoles in each of its unit cell. Over a certain range of E , the polarization curve is similar to a linear dielectric; it has shallow slope, which is not shown in Figure 5. *This corresponds to the paraelectric behaviour and is totally reversible; polarization returns back to zero when the field is zeroed.*

Towards higher E values, e.g. on the order of several kV/cm for PVDF, the polar domains start to align with the field. This shows itself as a sharp increase in polarization P ,

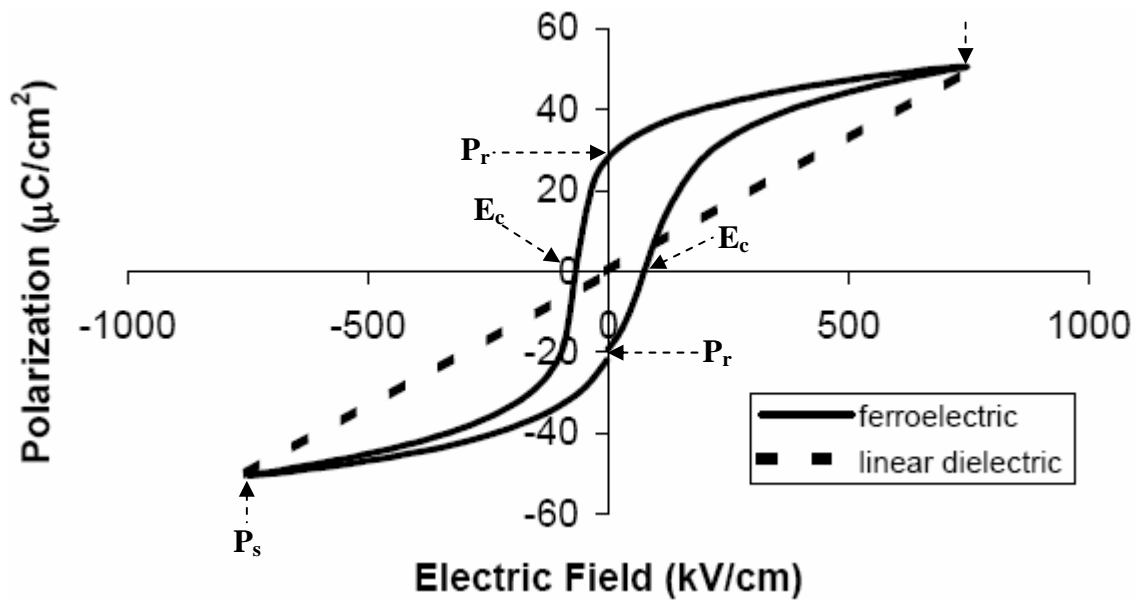


Figure 5 : A typical hysteresis loop for electric field vs. polarization compared with a linear dielectric response. Adapted from [39]

thus a high slope, meaning a high dielectric susceptibility (see Equation 2.1). Polarization P however can increase up to a certain value because almost all electric dipoles align themselves. This polarization state is called *saturation polarization* P_s , and changes from material to material.

Once the electric field is decreased gradually down to zero, the paraelectric component will be lost (see Figure 2) (as well as some ferroelectric contributions), but particular dipoles will preserve their direction, leading to *remnant polarization* P_r .

Upon reversing the direction of E , the existent polarization is first cancelled at a *coercive field* E_c , and a net zero polarization is again obtained. A **hysteresis loop** is completed once this process continued also for negative E values. The area within the hysteresis loop is proportional to the energy per unit volume that is dissipated once a full field cycle has been obtained.

2. MATERIALS PROCESSING

2.1 Electrospinning in Brief

Electrospinning is a high-voltage process that produces nanometer or micrometer-sized fibers both from synthetic and natural polymer solutions or melts. Production of polymeric fibers by electrospinning is first patented by Formhals in 1934 [48].

As defined by Doshi and Reneker the main mechanism in electrospinning is the creation of a charged jet of polymeric solution by an electric field [49]. As the jet travels in air the solvent evaporates leaving charged solvent-free continuous fibers, which are collected on a grounded plate. Through this, randomly oriented, high surface to volume ratio fibers, as well as various fiber morphologies and geometries are obtained, as noted in [50]. These are well interested in applications ranging from textile to composite reinforcement, sensors, actuators, biomaterials, filter and membrane technology [51].

One of the advantages of electrospinning is that polymers can be used both in solution and in melt form. To give a few examples; PVDF in its solution form is electrospun on a micro air vehicle wing skeleton, ending with a fibrous wing skin [4]. To be utilized in muscle cells and endothelial cell proliferation Mo produced P(LLA-CL) nanofibers [52]. Polyethylene fibers were produced by Larrondo and Manley [53]. Bombyx-mori silk fibers for textile applications were produced by Sukigara [54].

The home-made electrospinning setup depicted in **Error! Reference source not found.** is used in this study. It is composed of a GAMMA high voltage power supply, PUMPTERM Z100 syringe pump, and a conductive collector screen. A millimeter-sized syringe containing a PVDF solution is subjected to a potential difference between 5-15kV where the pumping rate of the syringe can be controlled via an RS232 unit (Uninventor 801 Syringe Pump).

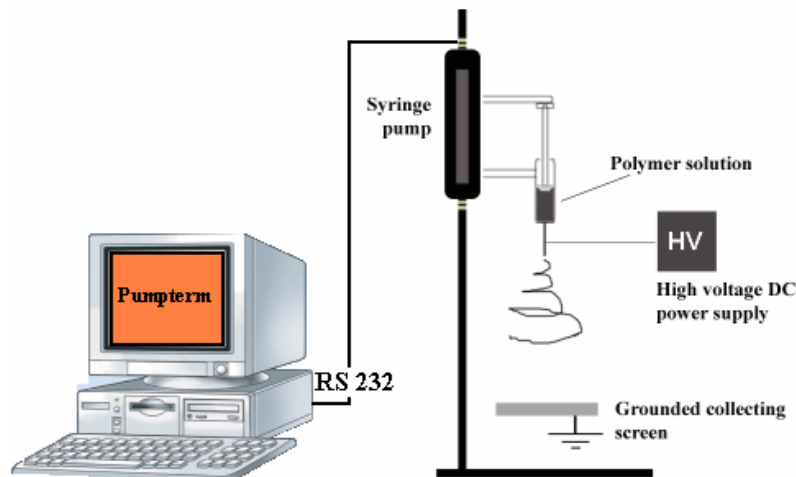


Figure 6 : The electrospinning setup.

2.2 Electrospinning of PVDF Fiber Mats

A short explanation on precursor solution preparation for producing PVDF fiber mats, as well as information about the electrospinning parameters used in producing these mats are explained in this section.

PVDF as the polymer is obtained from Alfa Aesar (MW > 500kg/mol, melt viscosity: 23500-29500 poise (230°C, 100/sec)), and N,N-Dimethylformamide (DMF) and acetone -as the solvents- are obtained from Merck Chemicals.

Using a PVDF+DMF solution lead to the formation of wet fibers and droplets on the collector, since DMF -as a low volatility solvent- did not quickly evaporate in air during electrospinning. The goal however is to produce dry fibers with uniform geometry. Due to this, even though acetone did not solve PVDF, acetone is mixed with DMF so as to increase its evaporation rate; thus, DMF+Acetone solution is after used as the solvent for PVDF. Moreover, different acetone/DMF ratios were tried to more optimize the produced fibers: 0%, 25%, and 50%. As a result, the solution concentration is decided to be 20% w/w (i.e. PVDF / (PVDF + Solvent Mixture)). A detailed study of this optimization procedure can be found in [19] and [55].

The other electrospinning parameter such as the applied voltage is kept between 8-12kV and the collector distance is kept between 15cm and 30cm [19]. As will be mentioned in section 4.1, these parameters caused changes on the crystallinity of the mats.

2.3 Electrospinning of ZnO Fiber Mats

The goal of this part is to fabricate ZnO fiber mats to be employed in a piezoelectric composite. In the next section ZnO/PVDF composites will be produced using these mats. Earlier presented work [19] gives a sufficient explanation about precursor solution preparation, which also briefly reported here. One can note, it is a relatively difficult process compared to the process of PVDF:

- Poly(vinyl alcohol) (PVA), at three different concentrations, is *very slowly* added into an Erlenmeyer flask containing distilled water until all of it is dissolved (to produce ZnO fibers with optimum geometry and morphology different solution ingredients were tried, as given in Table 1).
- Zinc acetate is dissolved in distilled water in a beaker to obtain a 35% w/w aqueous zinc acetates solution.
- Both solutions are heated up to 80⁰C when they get totally homogeneous.
- After waiting at 80⁰C for 5-10 minutes, the zinc acetate solution is poured *slowly* into the PVA solution and the final mixture is again kept stirring at 80⁰C for 5 hours.

Thus, each of the precursor solutions in Table 1 were electrospun at a potential difference of 9kV, flow rate of 25 μ l/min, and collector distance of 8cm. At the end, 4ml of the solution is electrospun on the collector (i.e. aluminum substrate). After the production, the polymer-ceramic precursor fiber mats were gently peeled off from the substrate and placed over two ceramic supports, as depicted in Figure 6, to after being put into the furnace.

Table 1 : Precursor solution and calcination parameters that were employed for the fabrication of ZnO fibers.

PVA		Zinc Acetate	
Mass (gr)	Concentration %	Mass (gr)	Concentration %
1.076	9.200	0.685	64
5.026	12.028	7.040	26
2.504	12.000	2.585	35.5
3.336	11.850	2.585	35

The supports were necessary for not leaving the mats touching the surface of the furnace, since otherwise they would be broken into pieces. The reason for this is shrinking of the mats -due to the burn-out of organic material in the precursor- and consequently the friction occurring between the mat and the surface of the oven.

Following the sample preparation, a two step heating process is programmed into the furnace (Protherm PLF Commander 100), as depicted in Figure 7: The sample is initially heated up to 120°C and kept there for 1 hour to get rid of its moisture. Then, it is further heated to 500°C at a rate of 0.5°C/min to make all organic compounds burn, and be left with a ZnO fiber mat.

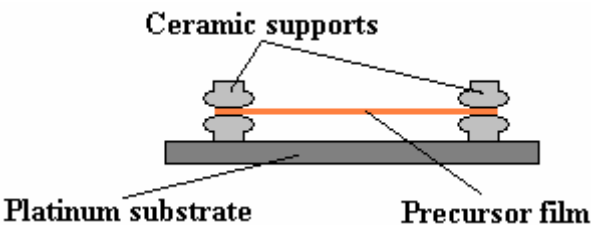


Figure 6 : Schematic representation of sample preparation for calcination process.

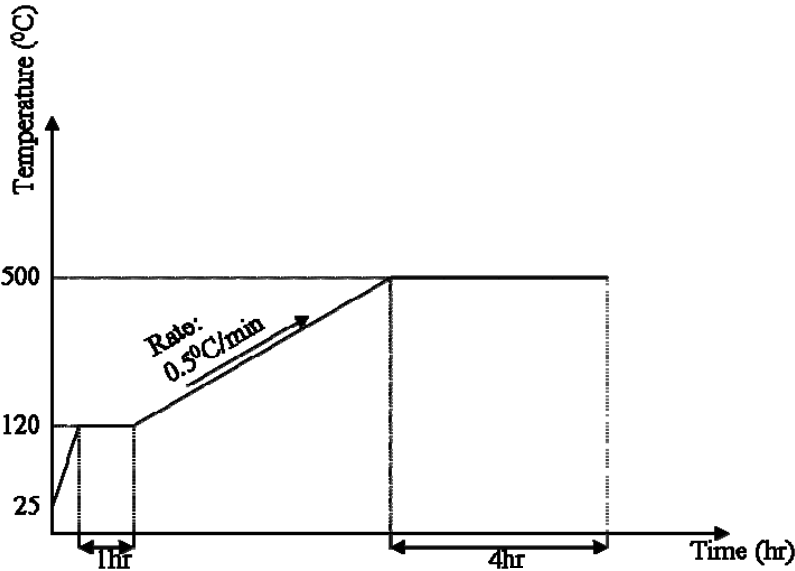


Figure 7 : Heating method for the calcination of polymer/acetate precursor fibers to produce ZnO fibers.

2.4 ZnO / PVDF Electroactive Composites

This section aims at fabrication of a smart material system composed of ZnO and PVDF. The idea of the composite material system is on account of the complementary characteristics ZnO and PVDF for flexibility and piezoelectric activity.

The system includes PVDF as the flexible piezoelectric polymer and ZnO as the piezoelectric ceramic; brittle, but capable to respond strains without poling. Two alternative processes were investigated. The first process made use of ZnO fibrous formation achieved by calcining PVA/zinc acetate precursor fibers via electrospinning. The second process employed commercial ZnO nanopowder material having wurtzite structure. This suggested the ZnO ingredient in the system should impart piezoelectricity without poling.

The free standing composite pellets with electrodes on the top and bottom surfaces were then subjected to sinusoidal electric excitation and response is recorded using a fonic sensor.

Former to explaining the processes, it will be helpful first to introduce the process flow for both the fiber-based and powder-based composite, as in Figure 8.

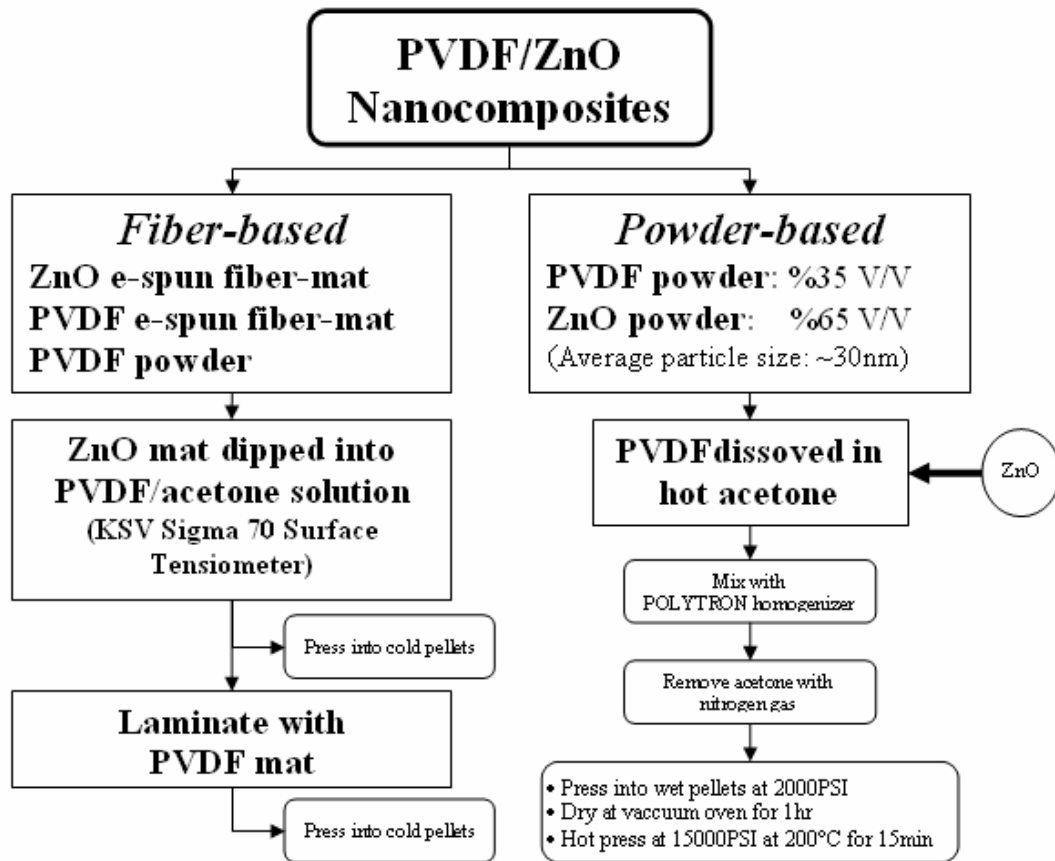


Figure 8 : Process flow for fiber-based and powder-based production.

2.4.1 ZnO Fibrous Mat/PVDF Fiber-Matrix Composite

ZnO fibrous mat is dipped into a PVDF/acetone solution by KSV Sigma 70 Surface Tensiometer. Acetone is chosen because it evaporated faster than DMF. To make PVDF penetrate into the mat sufficiently, the mat is kept inside the solution for one day. The viscosity of the solution is chosen by trial and error. When viscosity is not large enough voids between the fibers were poorly filled; if it is more than enough, the highly brittle mat either broke into pieces during dipping or absorbed the PVDF solution very hardly, resulting again with poorly filled voids. After the dipping operation the resulting composite is left in an oven at 50°C for 1 day to force acetone evaporate. The resulting composite is shown in Figure 9.

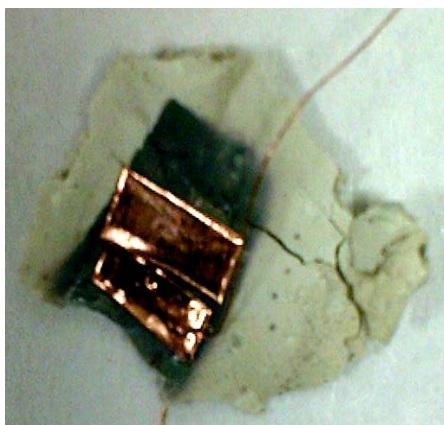


Figure 9 : A part of ZnO fiber mat dipped into PVDF solution after acetone has evaporated.

2.4.2 ZnO Fibrous Mat/PVDF Fibrous Mat Composite

Another pellet is pressed by sandwiching electrospun PVDF fiber mats between the PVDF-dipped ZnO fibrous mat in order to increase the polymer content. Thus, a more flexible structure is obtained as seen in Figure 10. Note that the composite in Figure 9 could not be pressed into a pellet because it was still brittle to stand pressing unlike the sandwiched specimen in Figure 10.



Figure 10 : ZnO fiber mat sandwiched in between two PVDF fiber mats.

2.4.3 ZnO/PVDF Nanopowder Composite

The other way to produce a flexible piezoelectric composite is to consider the ingredients as nanopowders. For ZnO powder there was no preferred alignment direction within the material and aimed for uniform powder distribution.

In this process, ZnO (Inframat Advanced Materials, average particle size: ~30nm) and PVDF (Alfa Aesar, m.p. 155 -160°C) were utilized as powders. Through this method, a nanocomposite of %65 volumetric ZnO loading is produced.

Ceramic/polymer composites were prepared by first dissolving PVDF in hot acetone, placing ceramic nanopowder into this solution and mixing it for 5 minutes via a POLYTRON PT600 type benchtop homogenizer. Nitrogen gas is introduced after to remove acetone until a gel-like soft paste is obtained, and this paste is pressed into wet pellets using a Specac pellet press at a pressure of about 2000 psi. After drying the composite in vacuum oven at 100°C for 1 hour, the pellet is hot-pressed at 200°C for 15 minutes at about 15000 psi [29]. The resulting pellet is shown in Figure 11.



Figure 11 : ZnO/PVDF nanopowder composite pressed into a pellet.

3. ELECTROMECHANICAL CHARACTERIZATION

3.1 Measurement Setup

Measurements were performed using a setup composed of a high voltage supply/amplifier (TREK 610E) driven by a function generator, a high resolution fonic sensor (MTI-2100) with a sensitivity of $0.00042\mu\text{m}/\text{mV}$, and a National Instruments data acquisition system.

The fonic sensor's structure and working principle can be summarized as follows: The probe tip consists of a number of randomly oriented light transmitting and receiving fibers where the light source is a regular halogen lamp. The transmitting fibers carry the photons, which in operation hit on the sample surface after which some of them reflect back to the receiving fibers. The sensor electronics then converts these into Volts. In order to get displacement data, the output is multiplied by the sensitivity of the probe. This sensor has a resolution up to 2.5\AA and a frequency response from 0Hz to 500 kHz. A guiding study concerning the piezoelectric characterization of bulk and thin-films can be found in [56]

The whole measurement setup is shown in Figure 12, Figure 13, Figure 14 and Figure 15, and its working procedure is as follows:

1. A down-scaled value of amplitude and the actual frequency values of the real signal are assigned to the function generator. The function generator drives the amplifier.
2. The amplifier's outputs are connected to the sample in order to drive it.
3. The fonic sensor senses the sample displacement and interprets it as Volts, which can be acquired via its BNC-type analog output.
4. The analog output of the sensor is connected to one of the analog inputs of the data acquisition system and therein filtered.

5. In order to observe the input and output signals altogether, the amplifier's "voltage monitor" output is also connected to one of the analog inputs of the data acquisition system
6. The measured signal can be displayed using one of "Scope" blocks or recorded via the LabView software.

At high voltage requirements ($>100V$), for example when electrostrictive activity would be detected, the amplifier is used together with the function generator. At low voltage requirements however ($<10V$), since the amplifier provided quite a noisy output the films were driven only by the function generator.

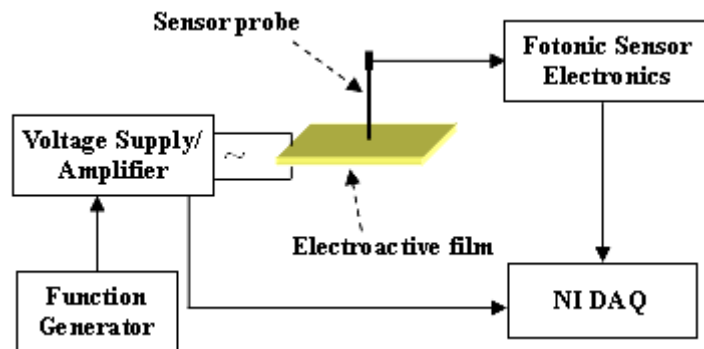


Figure 12 : Schematic representation of the electroactivity measurement set-up

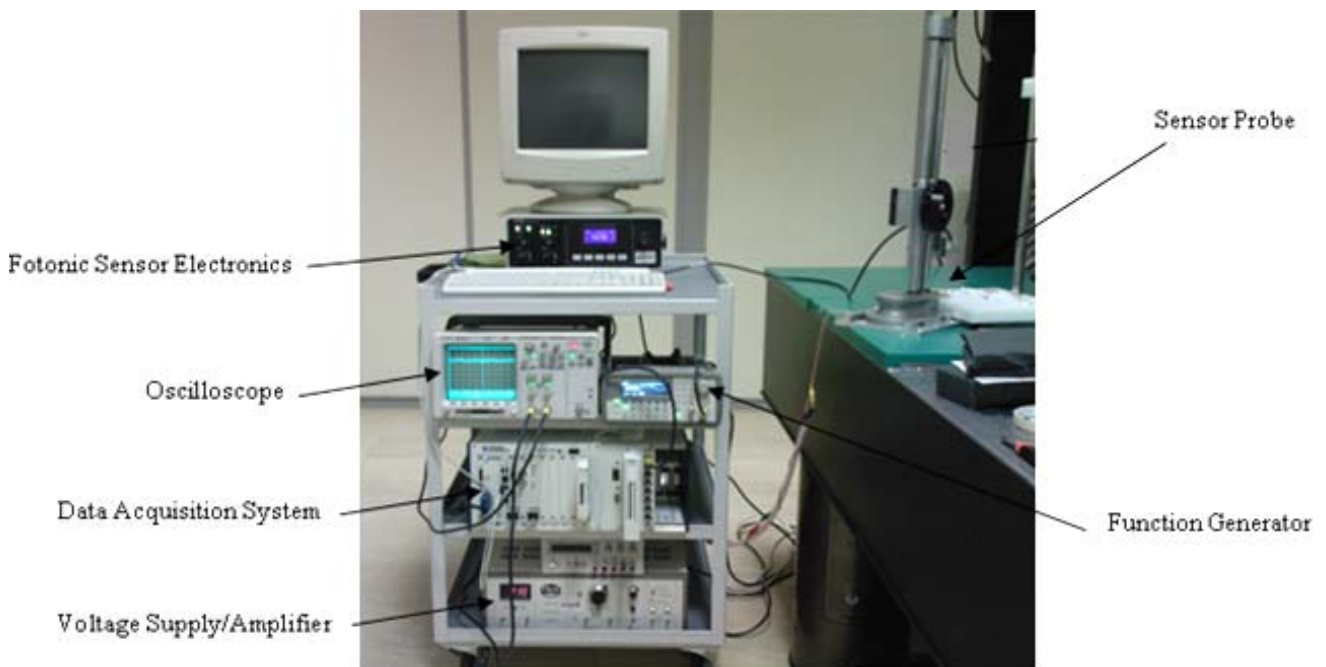


Figure 13 : Electromechanical measurement setup.

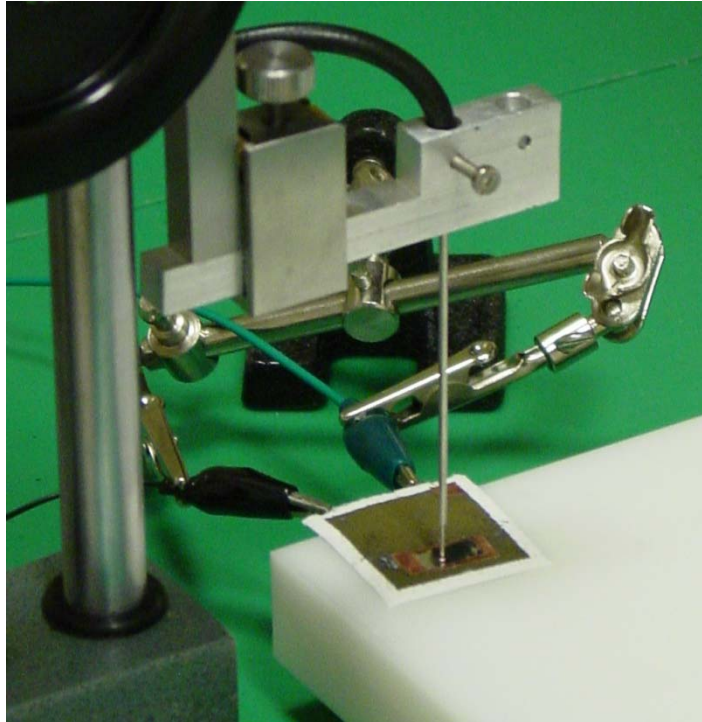


Figure 14 : Electromechanical measurement setup: A closer view to the photonic sensor probe together with the specimen.

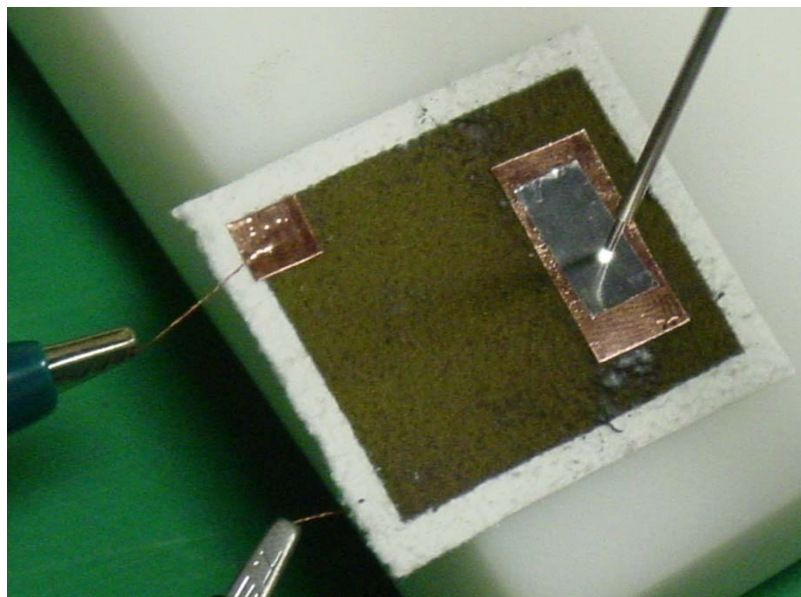


Figure 15 : A picture of a gold-electroded PVDF electrospun mat at the time of a measurement. Copper and aluminium films are adhered just below the sensor probe for the sake of reflectivity and noise-free signals.

Lastly, note that the figures showing the photonic sensor output in the below sections will have no “Strain Response” labeled axis -despite generally the strain responses are discussed-; but instead they will have an “Output Voltage” labeled axis. Since “Output Voltage” corresponds to the photonic sensor’s voltage output, which is linearly proportional to strain,

only numerical values change due to a correction factor between voltage and strain, but the response characteristics remain the same.

3.2 Coating and Sample Preparation

This section concerns in coating patterns applied to the processed materials and sample preparation study, which makes them ready for electromechanical measurements. Noteworthy to say that *the tasks were primarily planned and performed to search for the existence of piezoelectricity in PVDF fibrous mats, but the procedures converged through the efforts described below can be applied in the characterization of ZnO or other electroactive materials.*

In advance to the measurements an evaluation has been made among silver and gold for their use as the electrode material. The requirement is to yield with a reflective surface sufficient for the fonic sensor to make relatively sensitive and effortless measurements. Conductive coating is done on PVDF electrospun mats' surfaces using a vacuum evaporator (EMITECH-K950X) by gold and silver targets (EMITECH-K350). Consequently, the tests revealed that the gold target yielded more reflectivity on surfaces composed of fibrous PVDF mats compared to the silver target. In fact, silver had provided adequately reflective surfaces with pellets made of ZnO nanopowders; however, it performed poorly when used with mats of fibers. Finally, gold is chosen as the coating material because it allowed good usage both in regular films and fibrous mats.

In the two cases below it is assumed that there existed net permanent electric dipoles aligned along the thickness (Case 1) and along the length of the samples (Case 2). By conducting two different electrode patterns and associated electric field orientations verification of this assumption is sought. There were obviously two possible characteristics belonging to a PVDF mat; the first, piezoelectricity (due to permanent dipole movement), and the second, dielectricity (due to temporary dipole movement)- both of which caused a change in the dimensions of the film under an applied electric field. The efforts were aimed to find one(s) responsible for changing the film's thickness and length, separately.

Case 1: Investigation on through-the-thickness change: To reveal the type of dipole responsible for changing the mat thickness an electric field that would make the dipoles strain along its thickness were to be created. This is done by coating the top and bottom surfaces of

the mat and a creating a voltage difference between these coatings such that a through-the-thickness electric field vector is produced, either downwards or upwards, as seen in Figure 16 (during coating, since the fibrous mats were relatively thin, their near-boundary regions were masked by an adhesive tape to prevent arcing between their oppositely charged surfaces during actuation). This field vector resulted on a strain along the thickness of the mat and enabled to search for the dipole characteristics existing in the fibers' radial direction. The actual gold-electroded film is seen in Figure 17.

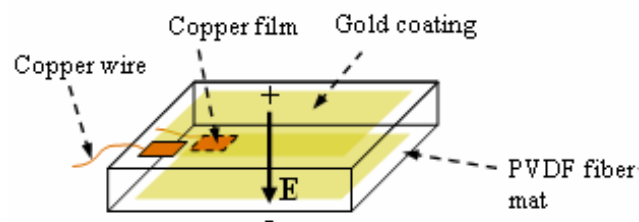


Figure 16 : First electrode format: Electric field vector is through-the-thickness.

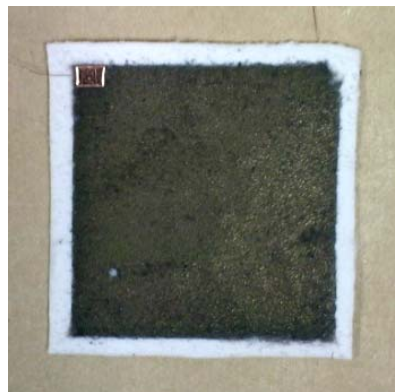


Figure 17 : Gold-electroded PVDF electrospun mat used for through-the-thickness change measurements.

Case 2: Investigation on in-plane dimensional change: To reveal the type of dipole responsible for changing the in-plane dimensions of the mat an electric field that would make the dipoles strain along its length were to be created. By coating two parallel electrode stripes on the surface of the mat and applying a potential difference, an in-plane electric field vector is created, as shown in Figure 18.

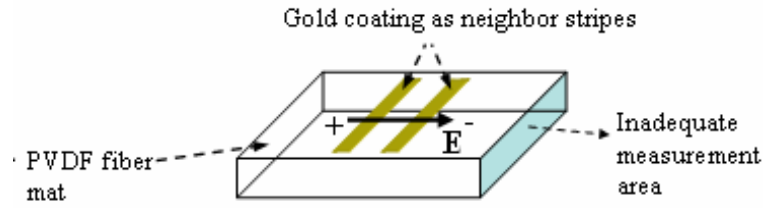


Figure 18 : Second electrode format: Electric field vector is in-plane.

In-plane strain, however, could not easily be measured by the available fonic sensor, and an additional step of specimen preparation is proposed. The reason for this is that the working area at the edge of the mat is a few hundred micrometers, which is not large enough for the light reflection to be sensed, as depicted in Figure 18. To create a larger area, the planar mat specimen is rolled into a tube, and a reflective film (Scotch Tape No. 850) is adhered on two ends of the new tube-like specimen as in Figure 19, and shown in Figure 20 and Figure 21. The dimension of the reflective film is chosen to be larger than the sensor tip's active diameter, which is $483\mu\text{m}$.

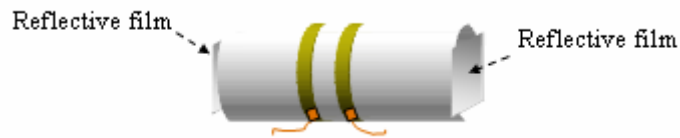


Figure 19 : Bent, tube-like specimen. The adhered reflective film created a sufficient working area for the fonic sensor probe.



Figure 20 : Gold-electroded tubular PVDF electrospun mat specimen used for in-plane strain measurements.



Figure 21 : The target surface of the tubular specimen.

Relatively detailed setups exist in the literature, which have generally been built to find piezoelectric strain coefficients. The aim here, however is primarily to determine and understand the nature of the electroactivity. In other words, the immediate interest at this point is that *how* and *why* the fibrous mat responded to an electrical stimulus, rather than *how much*. Therefore, the mats to be actuated were set up in a very simple manner that enabled us to detect the mentioned dynamics and plot the result quickly: The films were put on a teflon surface in a free-standing position, that is to say, without constraining any of their degree of freedom within any region or along any boundary. The only restriction to the movement of PVDF films is due to very thin conductive adhesive copper films mounted on PVDF's surface together with thin copper wires, as shown in Figure 16 and Figure 19. To hinder any unexpected vibration modes that these copper films would induce during actuation, they were cut in very small pieces, resulting in a surface area smaller than that of PVDF. Also during actuation the fonic sensor's probe tip is placed relatively far from them so as not to be influenced by the boundary effects.

3.3 Determination of the Nature of Electroactivity

The nature of electroactivity has been determined following two successive routes, which have been the basis for the measurements done in Section 4. In the first one, concerning PVDF mats, characterization was initialized from relatively high electric fields to determine whether the mats had a quadratic input-output relationship (i.e. being electrostrictive) or a linear input-output relationship (i.e. being piezoelectric or paraelectric). The results in Section 4.1.3.1 pointed out that at high electric fields, the mats possessed electrostrictive (quadratic) behaviour. Following this, in the second route, the applied electric field values were reduced and the characterization was focused on whether the quadratic

relation would be lasting. Consequently, it was observed that quadratic response diminished and a linear response started to dominate the behaviour. So, one had to determine which type of material property was responsible for this linear behaviour: Paraelectricity or piezoelectricity? The below “Possibilities” are based on this second characterization route.

Regardless of whether the applied electric field vector is through-the-thickness or in-plane directed the focus for all measurements below is on the direction of the strain vector ε relative to the electric field vector E -that’s direction is kept constant- as the orientation of the film’s surface normal n changed.

In Possibility #1, the sample is thought to be piezoelectric. Therefore, the polarization vector is named as *intrinsic* polarization, P_{intr} , since in piezoelectric materials polarization is a property belonging to the material’s internal microstructure: it exists even under no applied electric field. In Possibility #2 the sample is thought to be dielectric. There the polarization vector is named as *induced* polarization, P_{ind} , since in paraelectric materials temporary polarization is induced by an applied electric field.

As mentioned before, existence of radially-aligned dipoles (through the thickness of the mat) is investigated in the flat specimens, and axially-aligned dipoles (in-plane of the mat) are investigated in the tubular specimens.

Possibility #1: Piezoelectricity

At first the film is exposed to some value of E lower than its reported coercive field for commercial PVDF films. As a result, both E and P_{intr} are parallel and assumed to be in the same direction, and the film expands, as in Figure 22. Secondly, the film is flipped upside down to reverse P_{intr} (note that built-in P_{intr} presumed to exist fixed with respect to the direction of n) and now, P_{intr} and E are now in opposite direction and the film is supposed to shrink along the y-axis, as shown in Figure 23. Putting the film upside and downside makes a qualitative change on the measurement results: the film expands in the first case, but shrinks in the second case!

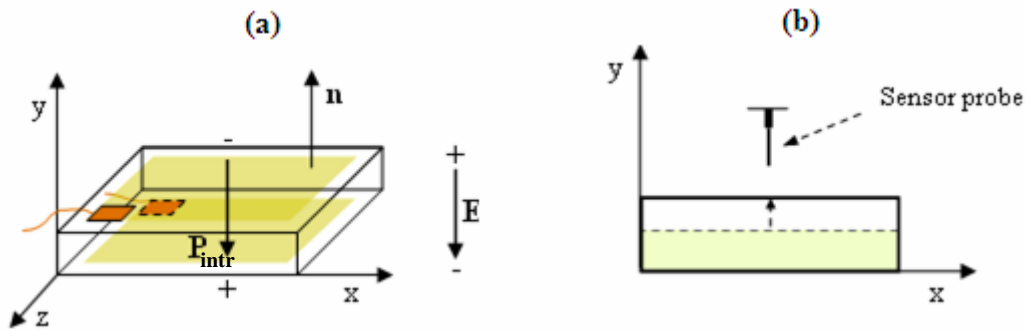


Figure 22 : Possibility #1: Piezoelectricity. Through-the-thickness configuration. (a) Directions of the electric field and intrinsic polarization vectors are the same; (b) as a result, the film expands.

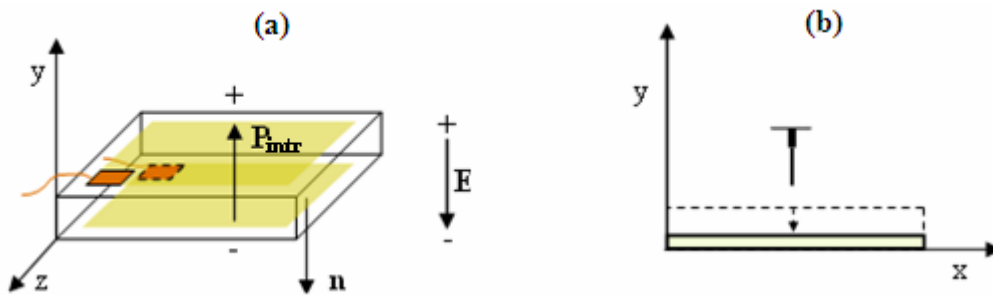


Figure 23 : Possibility #2: Piezoelectricity. Through-the-thickness configuration. (a) The film is reversed, so the directions of the electric field and intrinsic polarization vector directions are in opposite; (b) as a result, the film shrinks.

Possibility # 2: Dielectricity

Before starting the measurement, the film is reoriented for the direction of n to be the same as that in Figure 22. The film then is again exposed to the same E value and direction. As a result, both E and P were again in the same direction, and the film expanded, as shown in Figure 24. Secondly, the film is turned over (note that as supposed P in this case only depends on the direction of E , not n). Now, as before, P and E were over again in the same direction, and the film expanded, as shown in Figure 25. Putting the film upside or downside made no qualitative change on the measurement results: the film expanded.

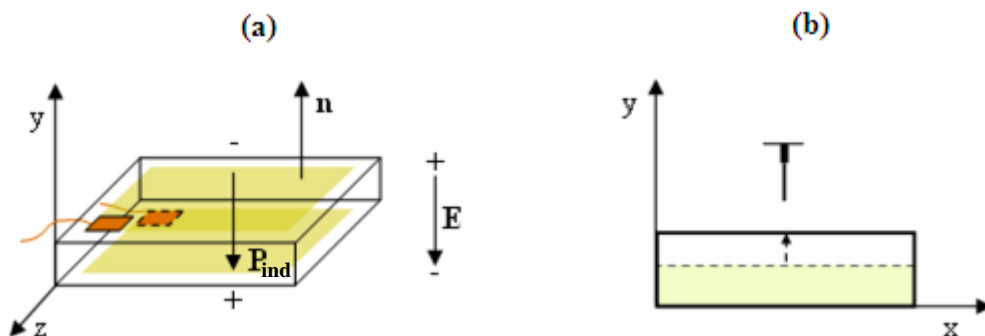


Figure 24 : Possibility #1: Dielectricity. Through-the-thickness configuration. (a) Directions of the electric field and induced polarization vectors are the same; (b) as a result, the film expands.

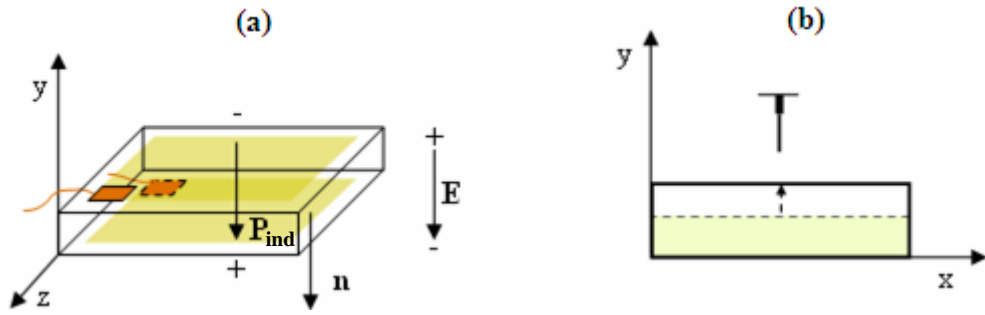


Figure 25 : Possibility #2: Dielectricity. Through-the-thickness configuration. (a) The film is reversed, however the directions of the electric field and induced polarization vector directions remain the same; (b) as a result, the film again expands.

The same arguments are valid also for the tubular specimens and described similarly in Figure 26 to Figure 29.

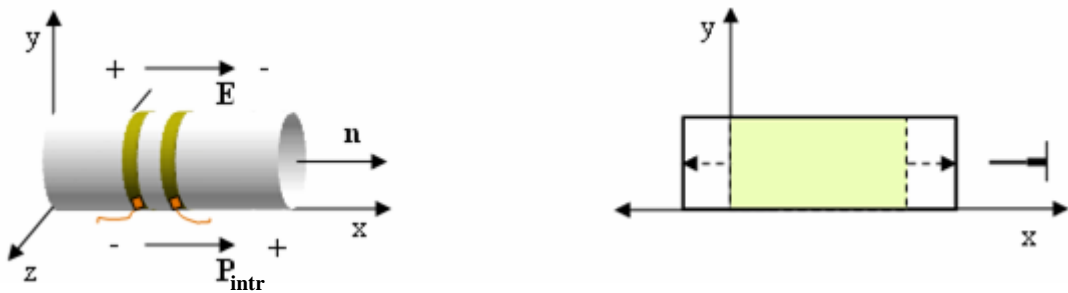


Figure 26 : Possibility #1: Piezoelectricity. Through-the-thickness configuration. (a) Directions of the electric field and intrinsic polarization vectors are the same; (b) as a result, the film expands.

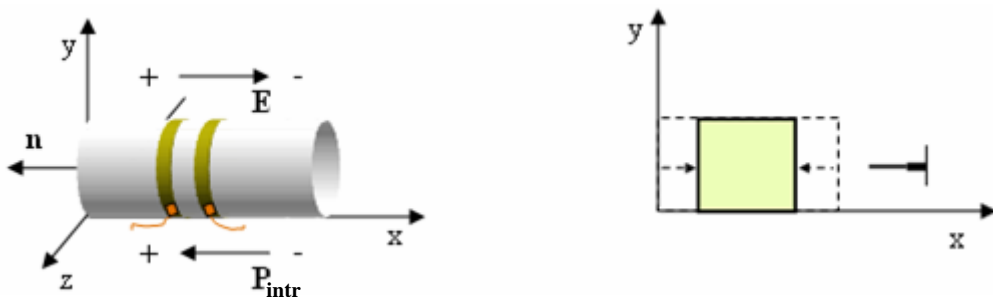


Figure 27 : Possibility #2: Piezoelectricity. Through-the-thickness configuration. (a) The film is rotated 180° around the y-axis, so the directions of the electric field and intrinsic polarization vector directions are in opposite; (b) as a result, the film shrinks.

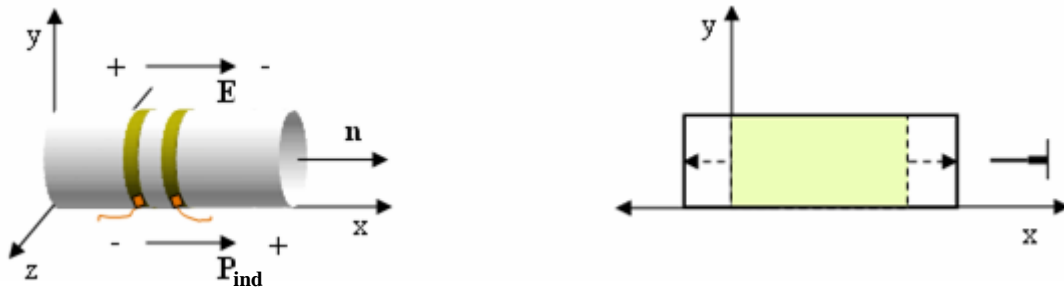


Figure 28 : Possibility #1: Dielectricity. Through-the-thickness configuration. (a) Directions of the electric field and induced polarization vectors are the same; (b) as a result, the film expands.

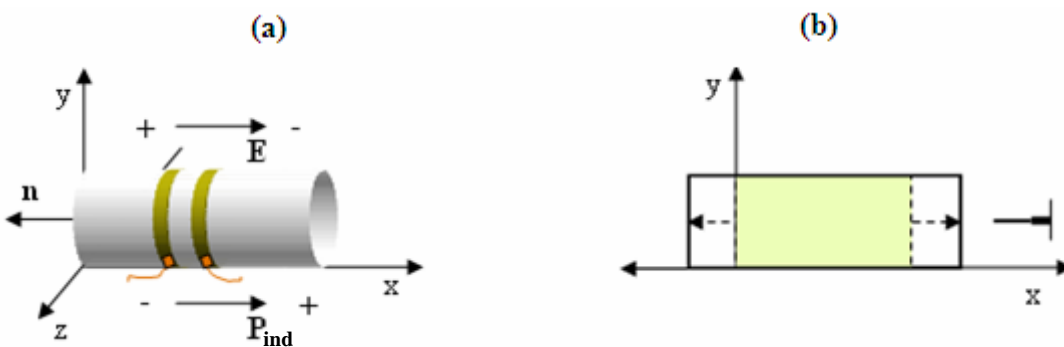


Figure 29 : Possibility #2: Dielectricity. Through-the-thickness configuration. (a) The film is rotated 180° around the y-axis, however the directions of the electric field and induced polarization vector directions remain the same; (b) as a result, the film again expands.

3.4 Faced Difficulties

Before coating and actuating the actual samples, i.e. PVDF fibrous films, we did a preliminary work on relatively less affordable ones, solution cast PVDF films, to face the bottlenecks in advance.

Electrode materials were chosen as graphite spray, copper tape and gold target as depicted in Figure 30 and the below processes were done:

- Graphite spray -purchased from Kontakt Chemie (Graphite 33)- is sprayed over the mask to coat the film.
- Conductive adhesive copper tapes -obtained from 3M- were cut and attached over the film.
- Gold target -from Emitech (TK8842)- is deposited for 12 minutes at 20mA deposition current. As a result, a gold layer of 70nm thickness is obtained [57].

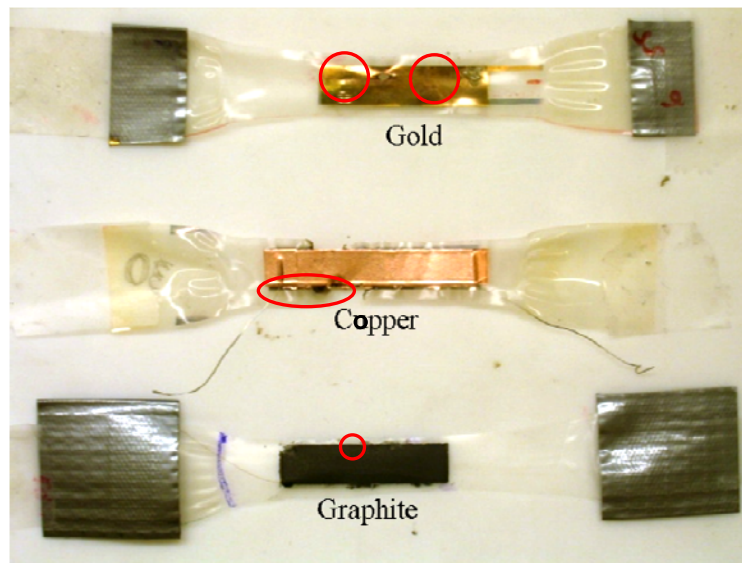


Figure 30 : Gold, copper and graphite coated samples exposed to electrode-pinning.

There is no difficulty during coating; but it aroused at the time of high-voltage actuation. As enclosed by red circles in Figure 30 the samples were exposed to electrode-pinning (i.e. wearing of the sample as small holes), which occurred due to charge accumulation/discharge at the film boundaries. This problem is overcome by

- Preparing cleaner samples free of oil, dust etc. on their surfaces
- Using samples with uniform surface morphology
- Using gold as the coating material rather than the others
 - Graphite spray is not resistant to charge accumulation. It evaporated, thus leaving uncoated parts at certain surface regions

Copper tape is very thick. Voltage breakdown occurred in the tape boundaries

4. RESULTS AND DISCUSSIONS

This chapter presents the results for XRD, DSC and electromechanical measurements of PVDF fiber mats, ZnO and ZnO/PVDF electroactive composites. XRD and DSC measurements are made in order to know the type and amount of crystal phase content in PVDF fiber mats, so that based on the results appropriate comments on the electromechanical measurement results could be made.

4.1 PVDF Fibrous Mats

4.1.1 XRD

Figure 31 shows that a PVDF fibrous mat -electrospun at 10kV and 22.5cm- has stronger α -phase characteristics than β -phase characteristics. The characteristic strong α -phase peaks are at 14.26° , 17.06° , and 18.86° -due to the reflections of (100), (020), and (110) planes-, and a weak peak at 25.88° . The mat also shows the characteristic strong β -phase peak at 20.72° , which is a reflection of (200) and (110) planes. Noteworthy to say, varying the voltage as well as the collector distance made no significant change in the intensity of the α and β -phases; thus Figure 31 is a representative result that is valid for all electrospun samples.

In addition, a crucial correlation between the samples electrospun at different voltage levels is determined: As the applied voltage increased an increase in β -phase formation happened, for large collector distances as seen in Figure 32. The reason for this is that the increasing voltage -thus the electric field- created an increased coulombic force and this force stretched the polymer jet more compared to a lower voltage level, thus enhancing the β -phase.

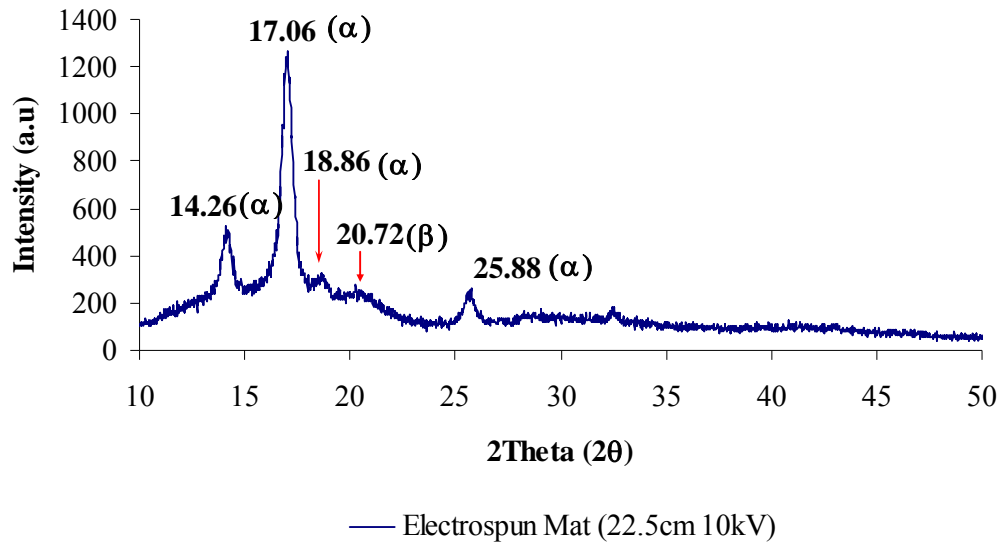


Figure 31 : XRD measurement results of PVDF electrospun mat.

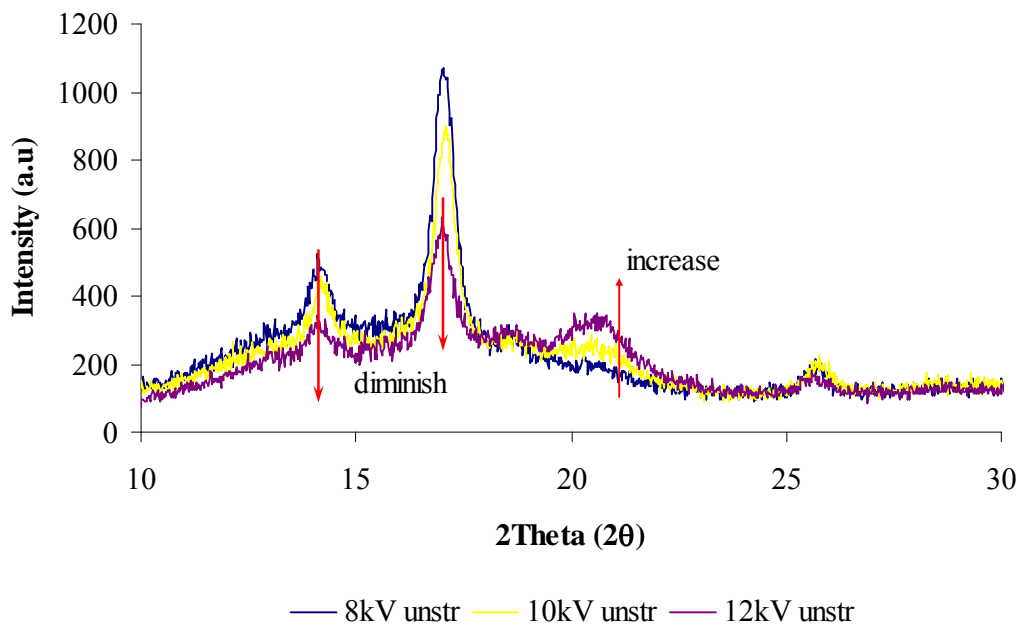


Figure 32 : Effect of electrical force on the fiber crystal structure.

4.1.2 DSC

In section 4.1.1, XRD measurements stated the correlation between applied voltage and β -phase intensity. The DSC measurements in this section state an additional outcome concerning the stretching effect. Comparing the measurements in Figure 33 done on *stretched* solution cast PVDF films in a previous study [19] and that of PVDF fiber mats, the shift that had occurred in solution cast films due to stretching also appeared in PVDF fiber mats. Note

that the enthalpy plot of electrospun PVDF perfectly fits onto that of the stretched solution cast PVDF.

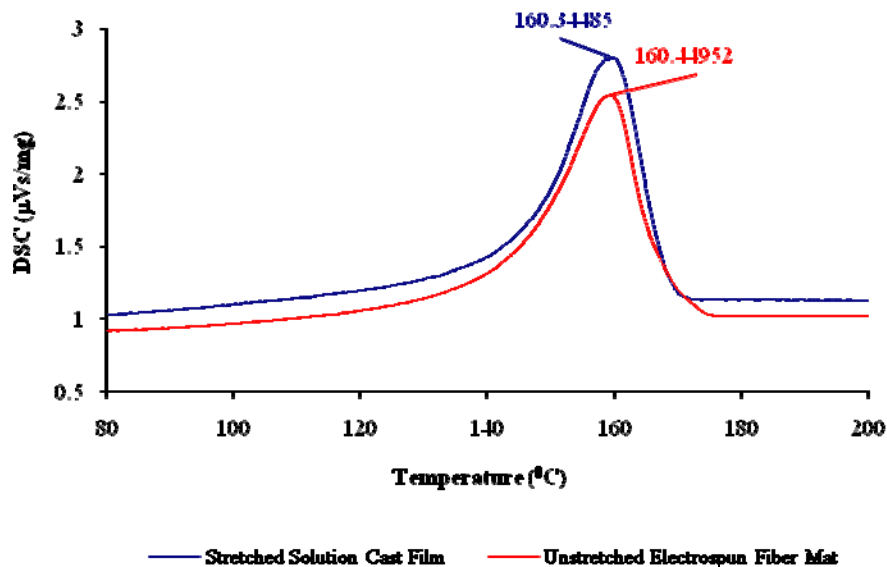


Figure 33 : DSC results of PVDF electrospun sample compared with a stretched PVDF solution cast sample.

4.1.3 Electromechanical Characterization

In this section, the direct electromechanical responses of the materials are reported.

4.1.3.1 Electrostriction in PVDF Fibrous Mats

Readings from the fonic sensor indicated that the electrospun PVDF fiber mat responded to applied electric field, as seen in Figure 34. The nature of the response, however, appeared to vary quadratic as a function of driving electric field that is interpreted as *electrostrictive* rather than piezoelectric. *This is evident from the fact that when the polarity of the input is switched to its opposite the sign of the output remained the same as in Figure 34a (Note the quadratic input-output relationship, as shown in Figure 34b).*

In conclusion, the measurement results downplayed the piezoelectric ability on as-produced electrospun PVDF fibrous films without poling and mechanical stretching.

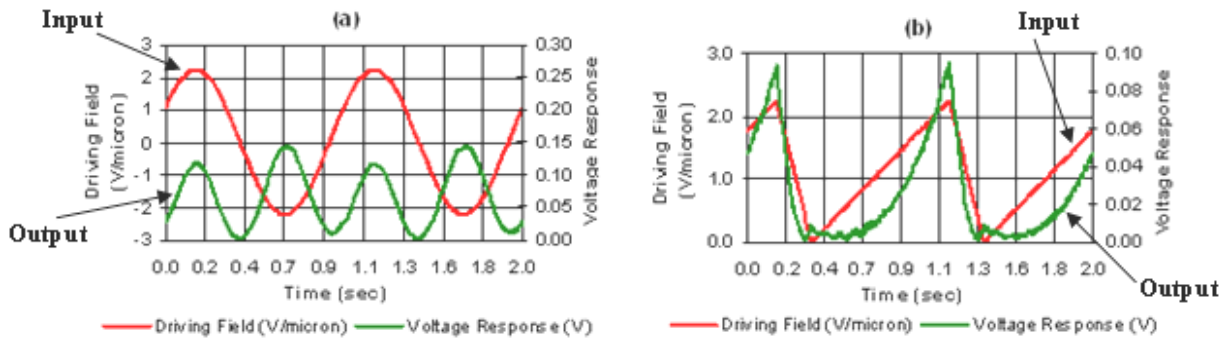


Figure 34 : Electromechanical response of as-received electrospun PVDF fibrous mats (100 μm thick) excited at 2000V, 1Hz. The displacement of the mats is approximately 0.042 μm . a) The sign of the output remained always negative even if the input's sign changed; b) quadratic relation exists between the output and the input.

4.1.3.2 Transition of Electrostrictive to Linear Dielectric Response

The below results represent the transition of electrostrictive to linear dielectric (i.e. paraelectric) response, which is determined by applying the methodology described in Section 3.3. A PVDF fibrous mat with 100 μm thickness is used and exposed to an electric field of 3.5V/ μm at 1.5Hz.

The measurements are again made by two electrode configurations. Out-of-plane strain occurs from the application of a sinusoidal voltage between the top/down coatings on the film, and in-plane strain occurs as a result of the two digitated stripes of electrodes.

The red-colored curves correspond to the input and black-colored curves correspond to the output.

4.1.3.2.1 Out-of-Plane Strain Response

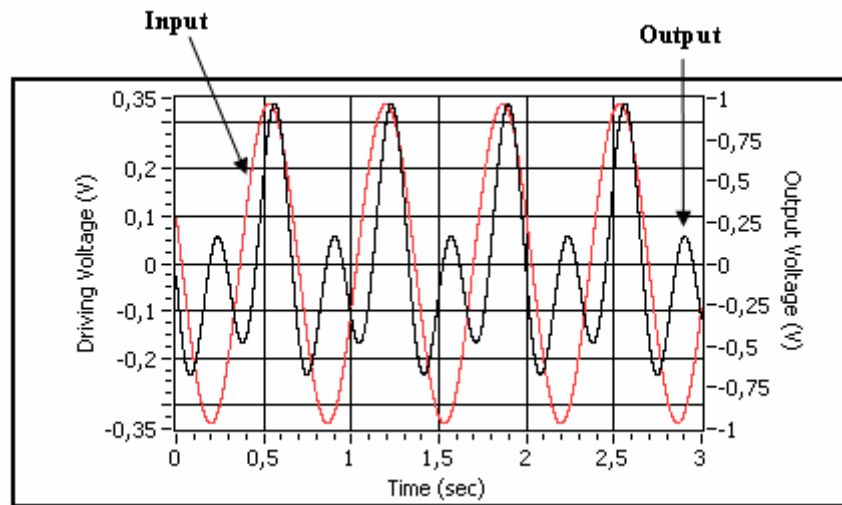


Figure 35 : Driving voltage is 350V at 1.5Hz. Sample thickness is 100 μm . A maximum displacement of approximately 0.71 μm resulted in the mats.

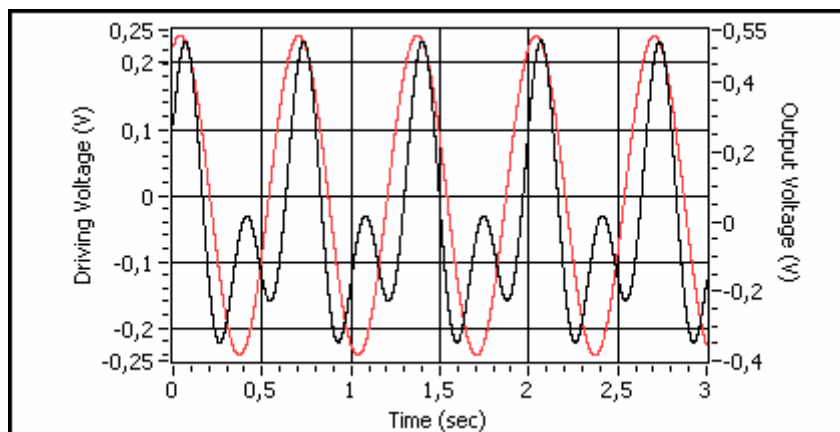


Figure 36 : Driving voltage is 250V. A maximum displacement of approximately 0.39 μm resulted in the mats.

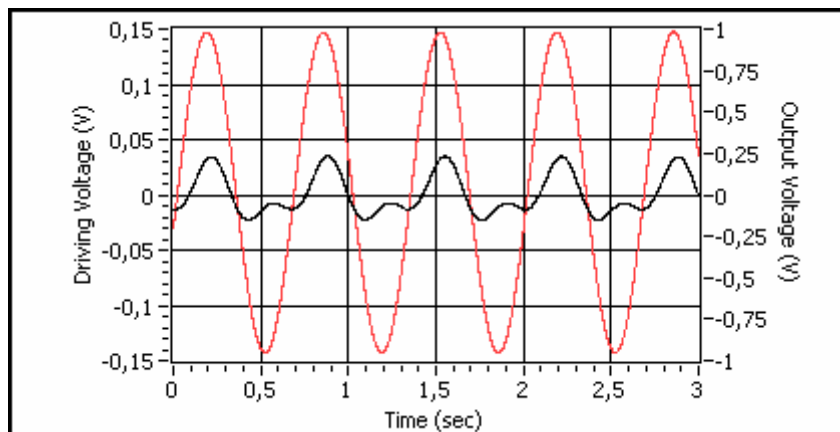


Figure 37 : Driving voltage is 150V. A maximum displacement of approximately 0.17 μm resulted in the mats.

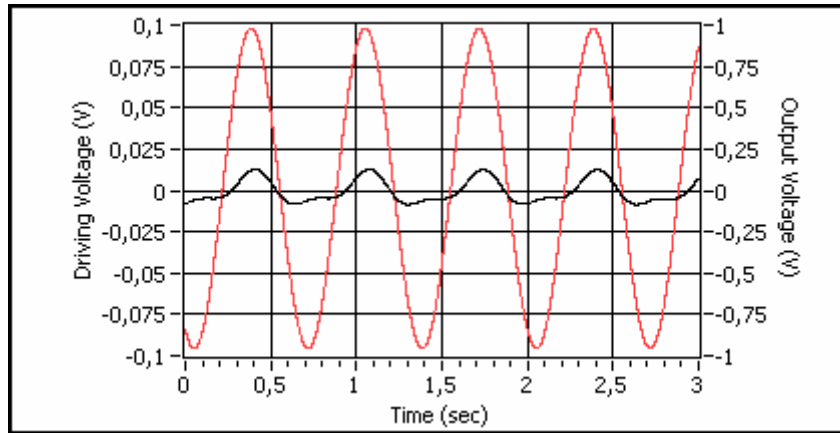


Figure 38 : Driving voltage is 100V. A maximum displacement of approximately $0.09\mu\text{m}$ resulted in the mats.

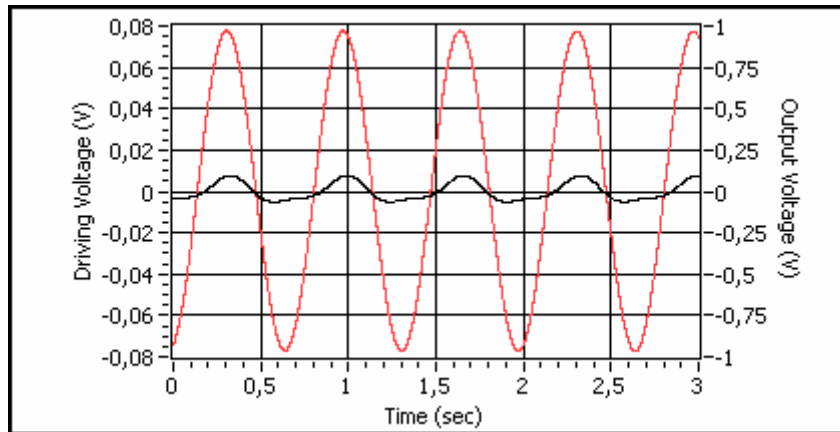


Figure 39 : Driving voltage is 80V. A maximum displacement of approximately $0.06\mu\text{m}$ resulted in the mats.

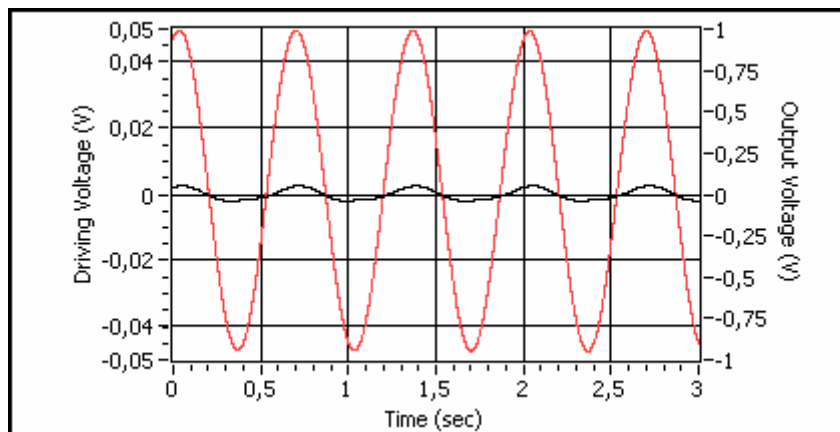


Figure 40 : Driving voltage is 50V. A maximum displacement of approximately $0.04\mu\text{m}$ resulted in the mats.

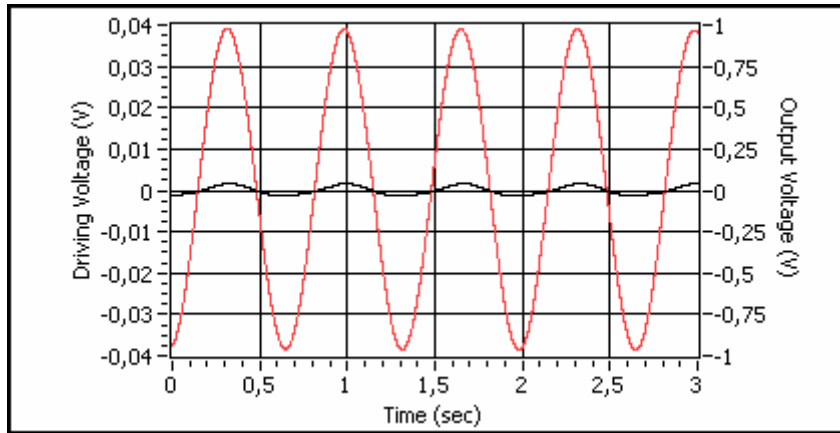


Figure 41 : Driving voltage is 40V. A maximum displacement of approximately $0.03\mu\text{m}$ resulted in the mats.

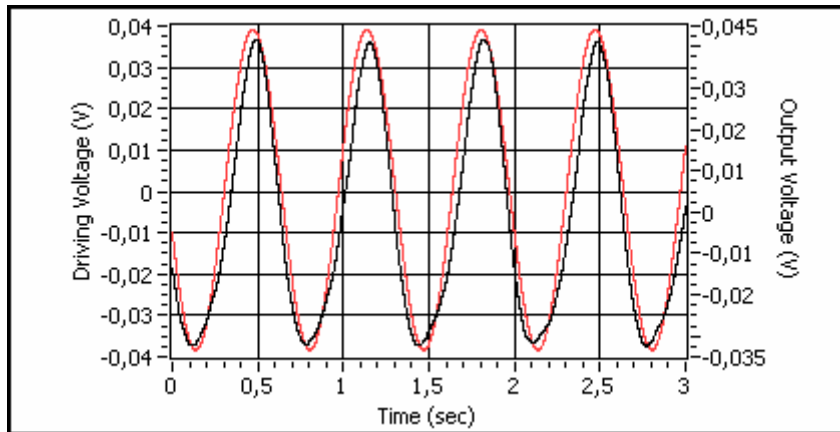


Figure 42 : Scaled version of Figure 41. A maximum displacement of approximately $0.03\mu\text{m}$ resulted in the mats.

4.1.3.2.2 In-Plane Strain Response

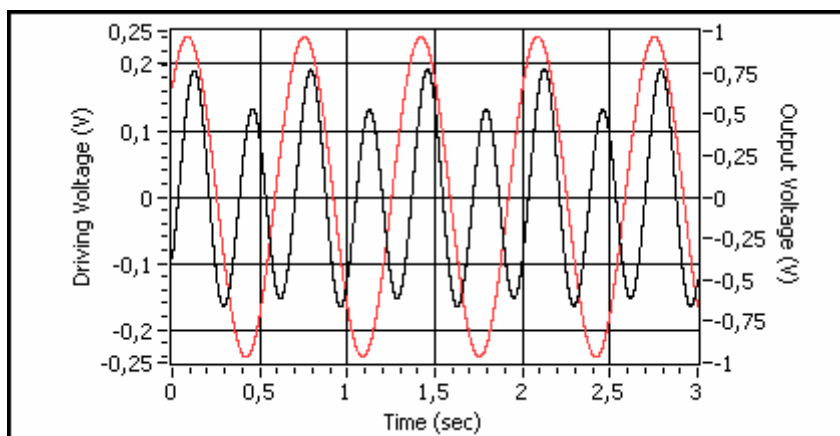


Figure 43 : Driving voltage is 250V. A maximum displacement of approximately $0.6\mu\text{m}$ resulted in the mats.

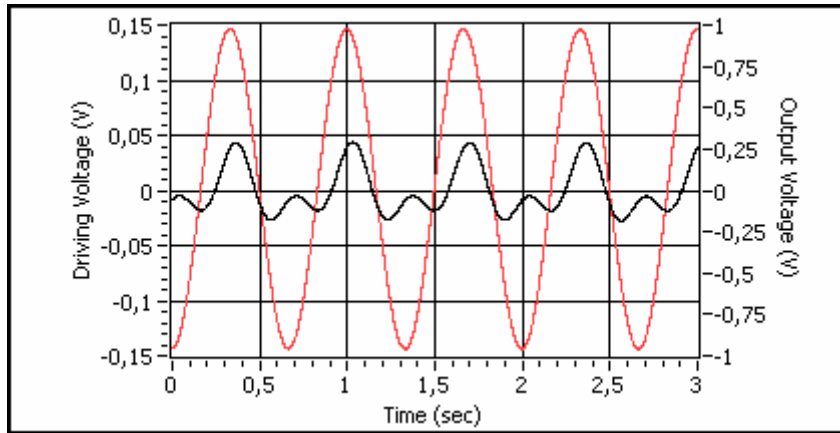


Figure 44 : Driving voltage is 150V. A maximum displacement of approximately $0.21\mu\text{m}$ resulted in the mats.

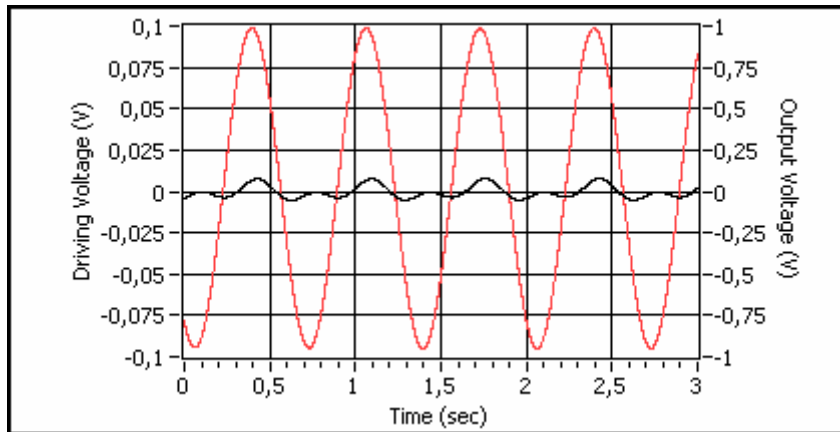


Figure 45 : Driving voltage is 100V. A maximum displacement of approximately $0.05\mu\text{m}$ resulted in the mats.

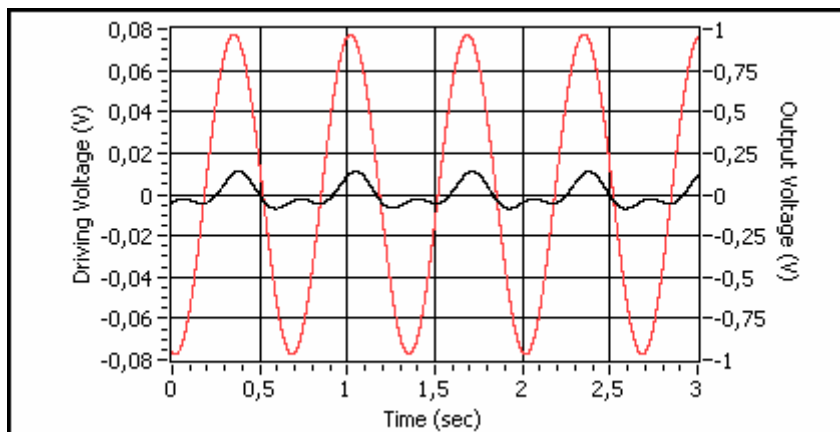


Figure 46 : Driving voltage is 80V. A maximum displacement of approximately $0.01\mu\text{m}$ resulted in the mats.

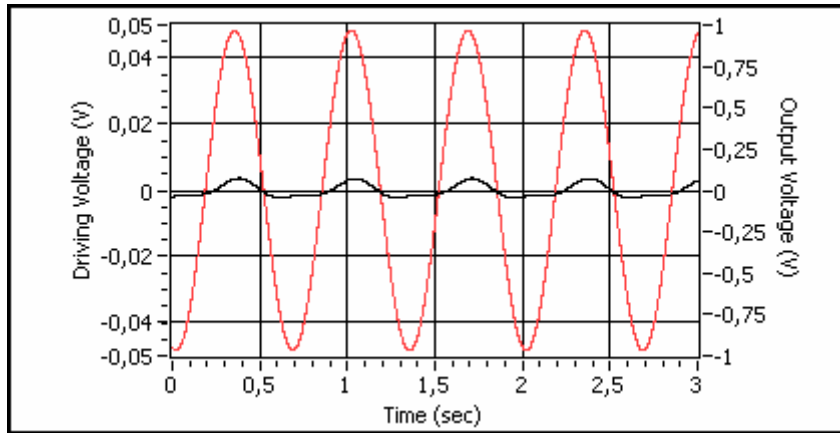


Figure 47 : Driving voltage is 50V. A maximum displacement of approximately $0.05\mu\text{m}$ resulted in the mats.

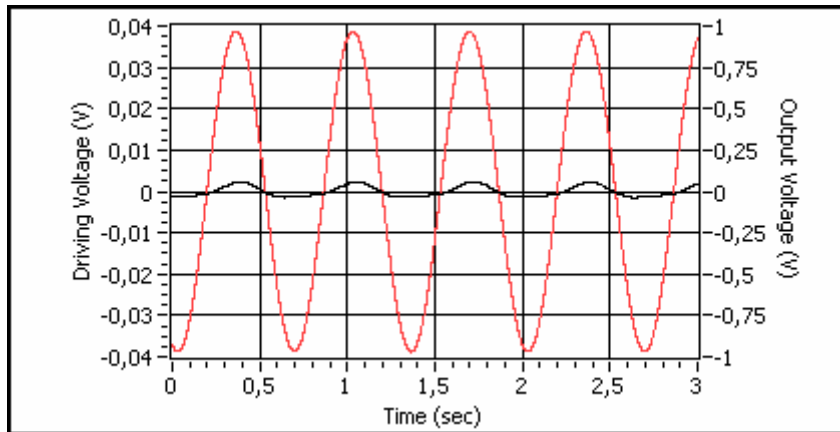


Figure 48 : Driving voltage is 40V. A maximum displacement of approximately $0.04\mu\text{m}$ resulted in the mats.

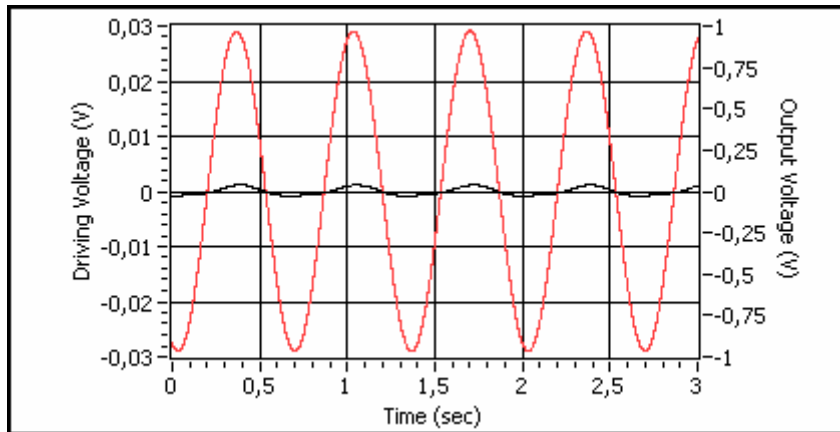


Figure 49 : Driving voltage is 30V. A maximum displacement of approximately $0.02\mu\text{m}$ resulted in the mats.

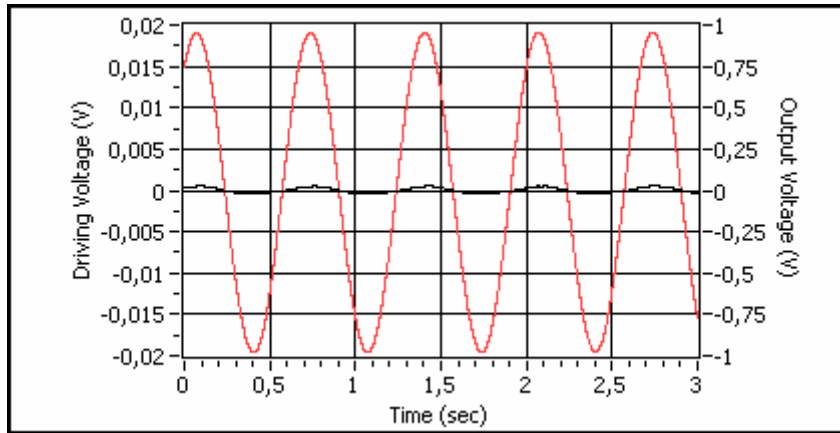


Figure 50 : Driving voltage is 20V. A maximum displacement of approximately $0.01\mu\text{m}$ resulted in the mats.

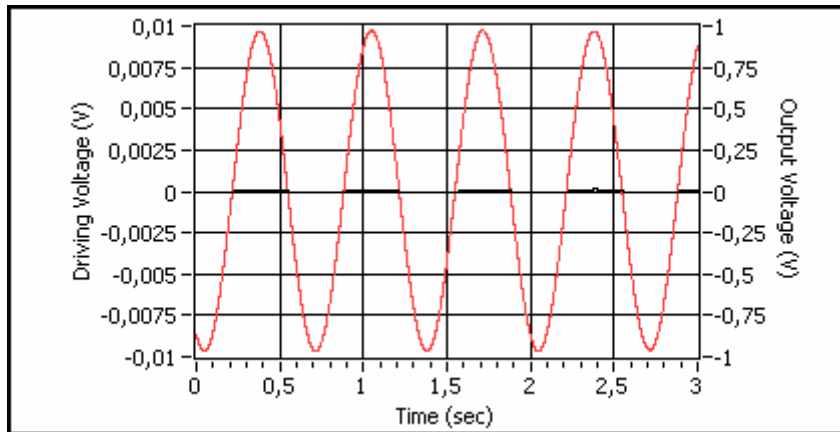


Figure 51 : Driving voltage is 10V. A maximum displacement of approximately $0.009\mu\text{m}$ resulted in the mats.

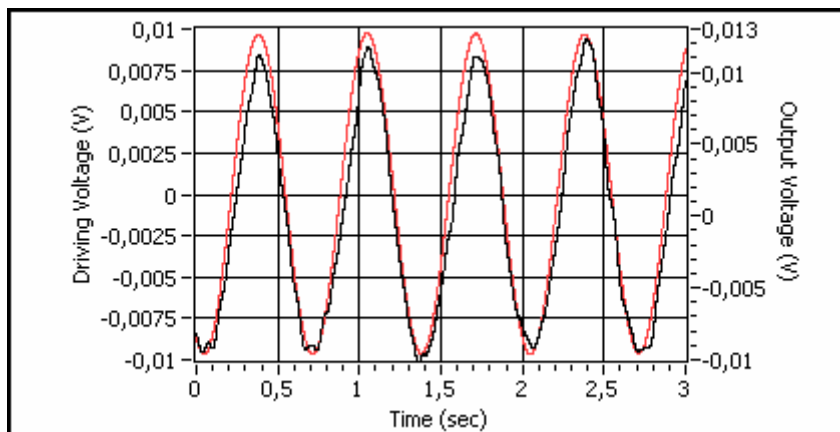


Figure 52 : Scaled version of Figure 51. A maximum displacement of approximately $0.009\mu\text{m}$ resulted in the mats.

4.1.4 More Investigations on the Linear Dielectric Behaviour of PVDF Fiber Mats

Note that the results depicted in section 4.1.3 are based on the mat's strain response, which is measured on its surface by an optical sensor. As these non-contact measurements on standing free specimens are thought to be sensitive to brightness and surface quality or waviness of the specimens, a supplementary evaluation for piezoelectricity rather ferroelectricity is also performed. Different electric field values were again applied on a mat as in the previous measurements; but this time the polarization (i.e. charges accumulated on the mat surface) is recorded by contact type measurement. The measurement setup consisted of Triangular electric field levels ranging from $2.5\text{V}/\mu\text{m}$ to $14.5\text{V}/\mu\text{m}$ were applied on a mat with a thickness of $200\mu\text{m}$.

The charge response in Figure 53 states that the PVDF electrospun fiber mat has a *lossy* behaviour up to approximately $15\text{V}/\mu\text{m}$, such that as the electric field increases the area enclosed by the polarization curve increases, and in addition, no hysteretic behaviour is observed. In Figure 54 the maximum-valued polarizations corresponding to each electric field level in Figure 53 are plotted to see if there exists any domain switching and saturation polarization.

At this point, it should be noted that the electric field values applied on the fiber mat are rather small compared to those applied on the commercial PVDF film, chosen as a reference sample, in which domain switching occurs at higher electric fields, as depicted in Figure 55. Consequently, one may infer that higher E fields should be applied to the fiber mats to let domain switching happen. It however is observed at high fields that the experimented fiber mats were exposed to dielectric breakdown even if the mats were dipped into oil, which is to fill the voids of air between the fibers and prevent breakdown. One of the possible reasons for the breakdown would be that the oil could not penetrate well inside the material and thus small voids of air may have remained during the experiments. This should further be investigated in the future studies in order to make more conclusive remarks that no domain switching occurs for higher E fields, and to correlate the results with that of induced via the fonic sensor experiments.

Despite the lower breakdown limit, it is an important result to see that the electrospun mat has the same behaviour as the commercial film up to a certain E field, which is approximately 15V/ μm as seen Figure 55.

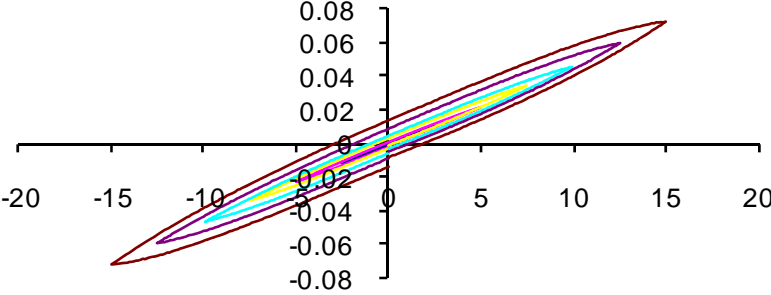


Figure 53 : Electric field (V/m) vs. Polarization (Q/m^2)

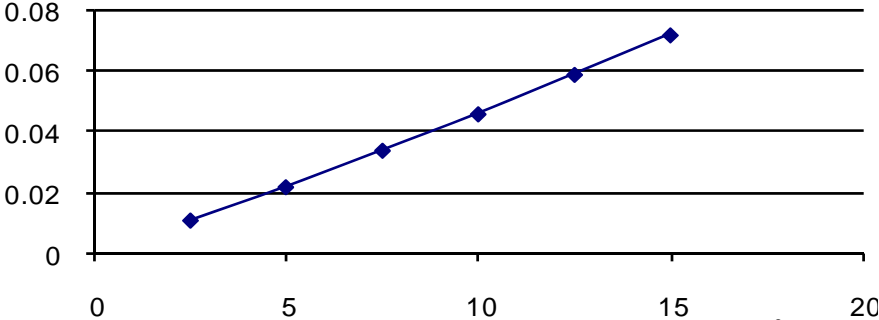


Figure 54 : Electrospun PVDF: E (V/m) vs. P_{max} (Q/m^2)

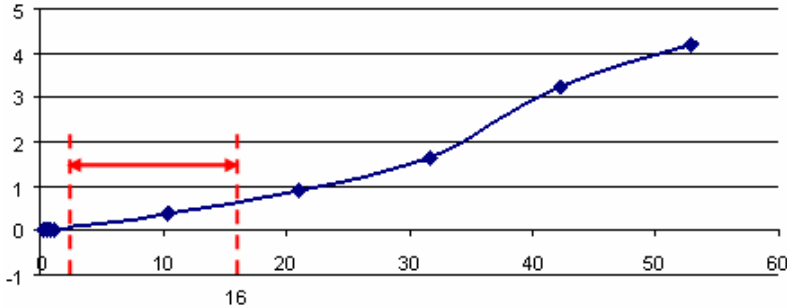


Figure 55 : Commercial PVDF: E (V/m) vs. P_{max} (Q/m^2)

4.1.5 Discussion on PVDF Fibrous Mats

Piezoelectric behaviour on electrospun PVDF fibers was expected because the two processes known as mandatory in achieving piezoelectricity from a PVDF materials system,

namely, mechanical stretching to enable β -phase conformation and electrical poling were thought to be intrinsically induced by electrospinning. The expectation comes from the fact that electrospinning uses a high voltage bias applied between the nozzle and the ground collector. The applied electrical force results in a stretching-like action, i.e. polymer chain alignment and elongation promoting β -phase while the polymer jet flies from the nozzle tip to the ground collector. The other process, poling, is expected to be induced with the electric field acting from the nozzle tip down to the collector as the fibers travel in air. Poling may also be induced with the field directed from the positively charged polymer jet to the negatively charged or grounded collector at the time the jet is in the vicinity of it, since the field reaches high values during this state. Focusing on these expectations, results obtained for PVDF fibrous mats can be discussed as follows

- 1) Applied potential difference was proven to be sufficient in promoting beta phase conformation that is required for piezoelectricity (Figure 32). As the DSC results in Figure 33 comparing stretched PVDF cast film and electrospun fibrous mat with coinciding melting points reveal that the electrospun fibrous mats may have dominant β -phase crystallinity even prior to stretching. It is however noted on Figure 32 that, although increasing applied voltage from 8 kV to 12kV increases the β -phase while drawing α -phase peaks down, dominance still seemed to be in favor of α -phase.
- 2) Because of the molecular chain alignment and elongation, in other words, stretching-like effect, electrospinning parameters such as the voltage magnitude and collector distance were chosen as 12kV and 22.5cm, respectively, the highest electric field among the tested in [19]. During electromechanical measurements, films produced at these process parameters were used.
- 3) A nonlinear electroactivity input-output relation as depicted in Figure 34, fit well by a quadratic approximation is labelled either as electrostrictive or electrostatic actuation. Latter type, however, requires relatively higher electric field levels than the applied electric field during measurements in this thesis, therefore, the recorded responses from Figure 35 to Figure 52 is interpreted as electrostrictive.
- 4) The electrostrictive behaviour in PVDF fiber mats is as expected in Figure 35; however is

only valid within a certain voltage interval. When Figure 35 to Figure 41 is step-by-step observed one may note that the film's response characteristics transforms to a rather different type as the driving voltage is brought to lower values. That is, positive-valued peak outputs resulting from negative-valued peak inputs diminish to zero, and afterwards go down to negative values

- 5) Subsequently, as shown in Figure 51 and Figure 52, at a very low actuation voltage of peak 10V negative-valued peak inputs now create negative-valued peak strains, not positive-valued ones. Although, this resembles piezoelectric characteristics -in which strain is directly proportional to the applied voltage- the film is in fact a pure dielectric - showing paraelectric dynamics. This was determined by the method explained in Section 3.3.
- 6) XRD and DSC results along with electroactivity measurements suggest that mechanical stretching and poling may still be required or much higher electric field values should be applied in electrospun mat production in order to attain piezoelectricity.

4.1.6 Faced Difficulties

Obtaining noise-free response is one of the most challenging parts of this study. At very small film strains the fonic sensor's analog output provided very low-amplitude signals compared to 50Hz electrical, high-frequency fluorescent and environmental noise. As an example, note the peak amplitude in Figure 52, which is only 13mV (*film's displacement is only 9nm!*). Two main problems faced were:

- **Calibration of the fonic sensor using the high-resolution probe**

The sensor had to be calibrated very precisely to end with proper results as well as clear signals. Since;

- Surface reflectivity of PVDF fibrous films is very poor
- The films never stand perpendicular to the sensor tip, which reduces the amount of reflected photons reaching the receiving fibers
- Active diameter of the probe tip is very small (483 μ m)

several places on the film must be searched for a sufficiently large reading on the sensor display (approximately 0.2-0.3V) so as to start the calibration.

- **Signal Conditioning**

Even the sensor owned high and low-pass filters, they were not adequate to provide a noise-free response. For this reason, high and low-pass filters of National Instruments' data acquisition system and LabView software were utilized as depicted in Figure 56. The low-pass filter is used to get rid of first of all the 50Hz noise, and the high-pass filter is used to remove the DC offset resulting from the sensor's electronics.

To give an example, for an input signal of 10V and 1.5Hz as in Figure 52, higher and lower cut-off frequency of the filters is set to 4Hz and 0.4Hz, respectively.

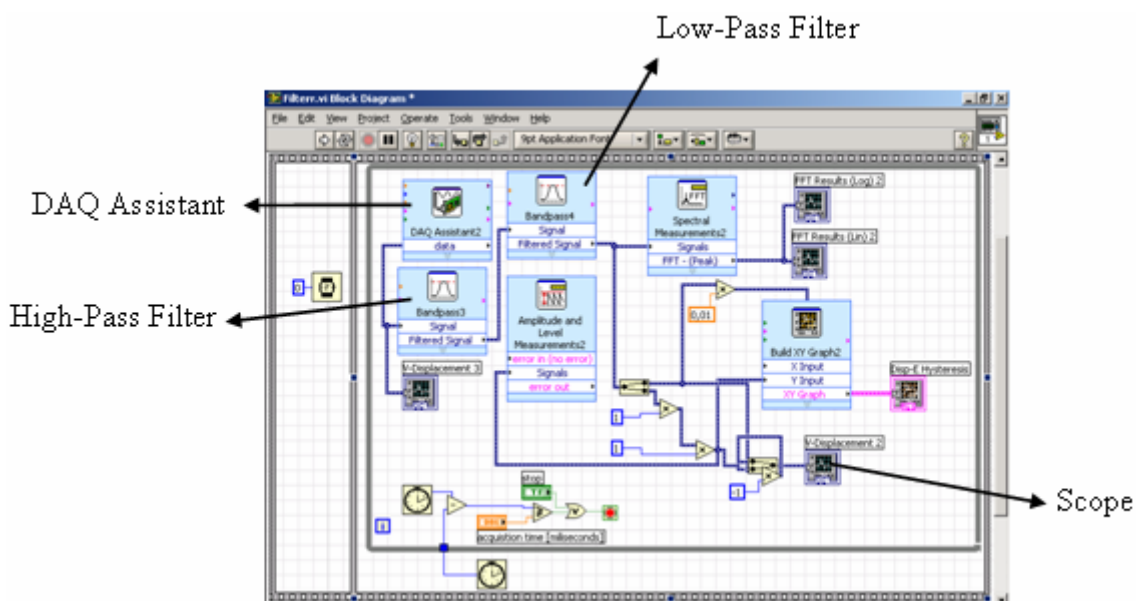


Figure 56 : LabView block diagram.

4.2 ZnO Fiber Mats

Resultant ZnO fibrous mats of 35% zinc acetate aqueous solution were further characterized by SEM. XRD is also used to figure out their crystal structure, that is whether wurtzite structure is achieved for ready-to-use piezoelectric properties.

4.2.1 Effect of Zinc Acetate Solution concentration

Zinc content affected morphology and structure of the precursor and ZnO fibers significantly as anticipated. Three different solution concentrations with different aqueous zinc acetate percentages were experimented, and a calcination procedure consisting two dwell temperatures as in Figure 7 is utilized. When the precursor solution contains high zinc

loading (50% zinc acetate aqueous solution) agglomeration is observed. Figure 57a is the SEM image of precursor fibers and Figure 57b is the fibrous network after calcinations. Note the agglomeration on the fibers.

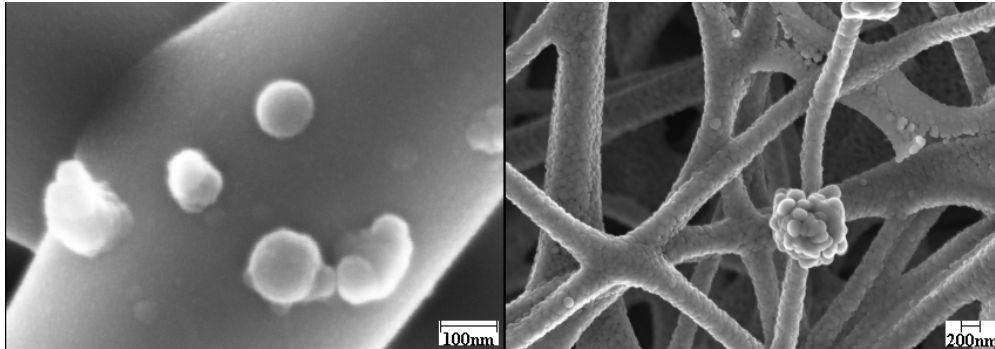


Figure 57 : Zn is the precursor solution with the highest zinc content. As it is seen in these SEM images, excess amount of zinc precipitates over both the precursor fibers (a) and the ZnO fiber itself after calcination (b).

Low zinc concentration (24% zinc acetate aqueous solution), resulted in mat of continuous uniform precursor fibers after electrospinning (Figure 58a). The calcined mat, however, did not form a fibrous network, instead broken pieces of ZnO fibers (Figure 58b). These two cases were considered as the two extremes here in terms of their resultant morphologies. Regarding the SEM images, PVA with 35% zinc content gave the finest results with a heating regime of $0.5^{\circ}\text{C}/\text{min}$ from room temperature up to 500°C . Therefore, zinc acetate aqueous solution concentration is fixed at 35% for further evaluation.

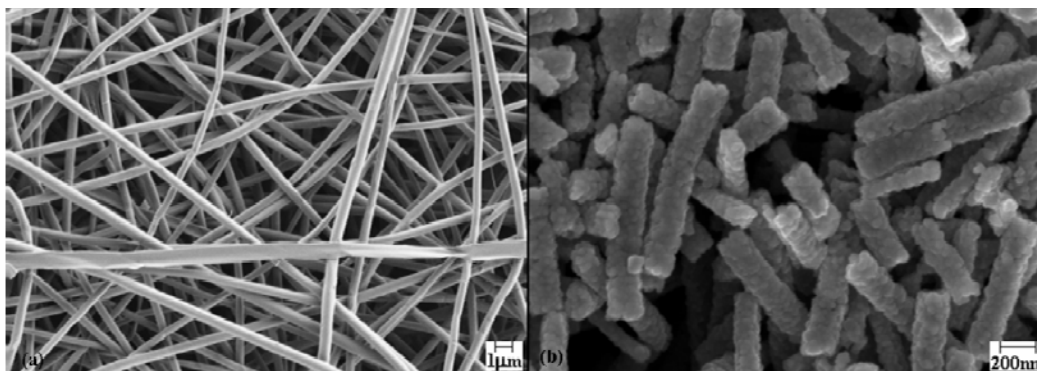


Figure 58 : (a) Zinc is the precursor solution with the lowest zinc content. The precursor fibers are uniform and continuous. (b) ZnO particles cannot always form continuous fibers; they mostly break into pieces due to small amount of zinc content.

4.2.2 Images by Scanning Electron Microscopy

Resultant ZnO fibrous mats of 35% zinc acetate aqueous solution were further characterized by SEM. XRD is also used to figure out their crystal structure, that is whether

wurtzite structure is achieved for ready-to-use piezoelectric properties. The produced precursor fibers by the process in section 2.3 were mostly precipitate-free, and uniform in diameter. Figure 59a is the SEM picture of these precursor fibers.

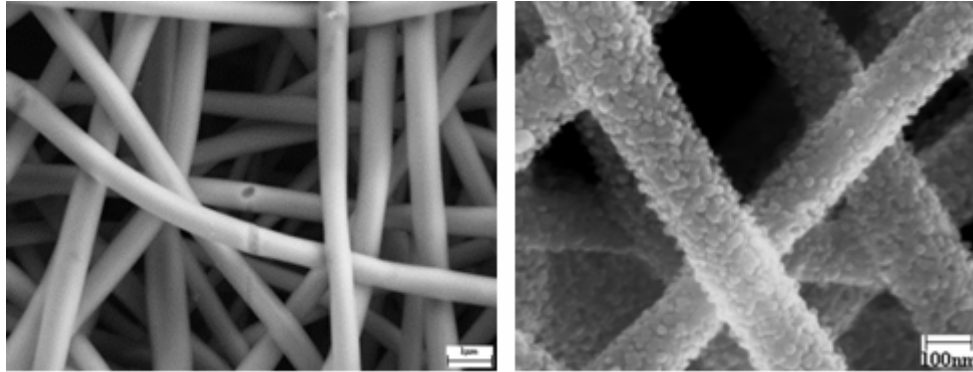


Figure 59 : (a) Precursor fibers; (b) ZnO sample imaged by 200K magnified. Grains with an average diameter of 20nm can be easily seen on the fiber structure.

High magnification SEM images of the ZnO fibrous formation after calcination (Figure 59b), however, reveal that the fibrous formations were composed of smaller spherical-to-hexagonal balls, say hexahedrons. These discrete particles (size of about 20 nm) in the elongated chain introduce physical drawbacks. When the fabricated mats were taken out of the furnace, it is observed that the resultant ZnO fibrous mat is fragile and difficult to handle; yet, the produced mat could lift its own weight. This mechanical weakness is attributed to the boundary morphology of the hexahedrons in the structure. The grain boundaries on the fiber work as cracks and the fracture of the mats occurs from those boundaries, making the ZnO fibrous mats fragile.

4.2.3 X-Ray Diffractometry

XRD measurements in Figure 60 confirmed exactly the desired crystallinity, which is the wurtzite structure. It is significant to observe this crystal structure, since the electroactive characteristics of ZnO comes from this specific crystal property. This property or electroactivity is sought in the composite made of the ZnO mat and PVDF as reported in the next section.

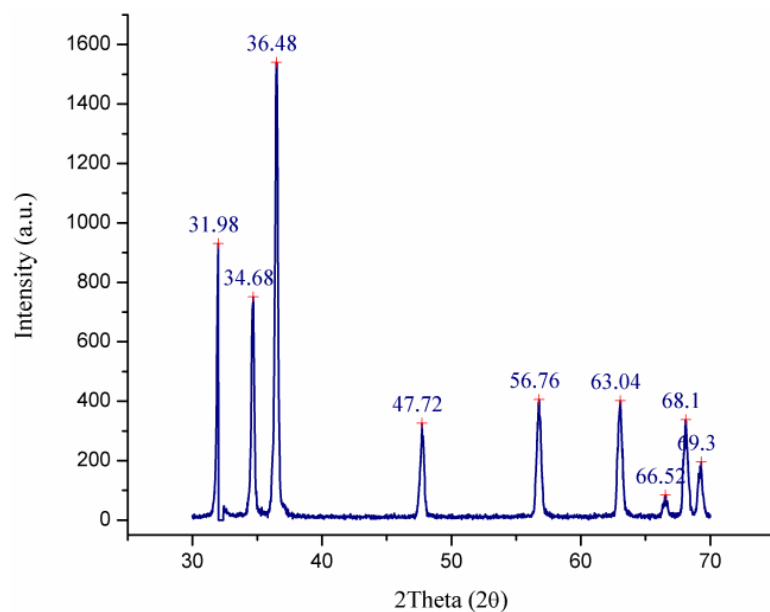


Figure 60 : XRD data obtained from ZnO samples. The peaks are similar to the characteristic peaks of the wurtzite structure.

4.3 ZnO / PVDF Electroactive Composites

4.3.1 ZnO Fibrous Mat/PVDF Fiber-Matrix Composite

The SEM images in Figure 61 and Figure 62 belong to a part of the pellet pressed from electrospun ZnO fiber mat dipped into a PVDF solution. Note that PVDF has filled in the voids between adjacent ZnO fibers to build *elastic bridges* between them. The resulting composite is relatively flexible -at least not brittle- compared to the ZnO fiber mats.

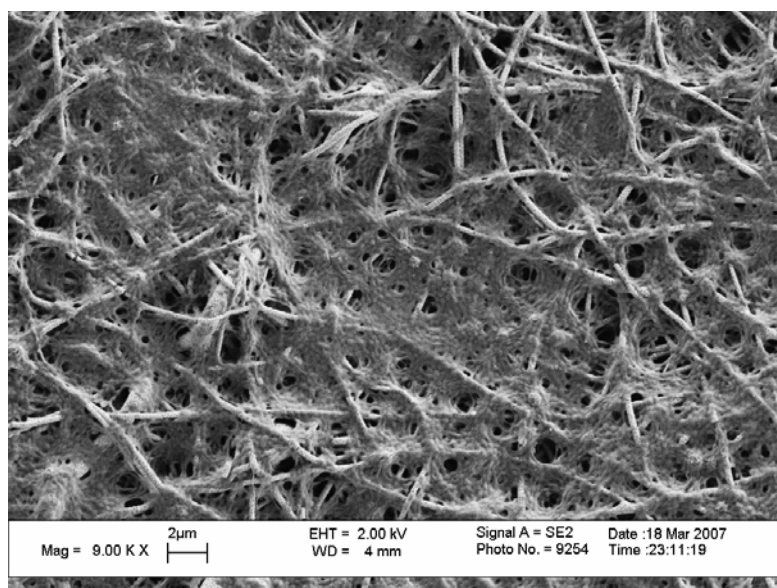


Figure 61 : SEM image of ZnO mat dipped into PVDF solution

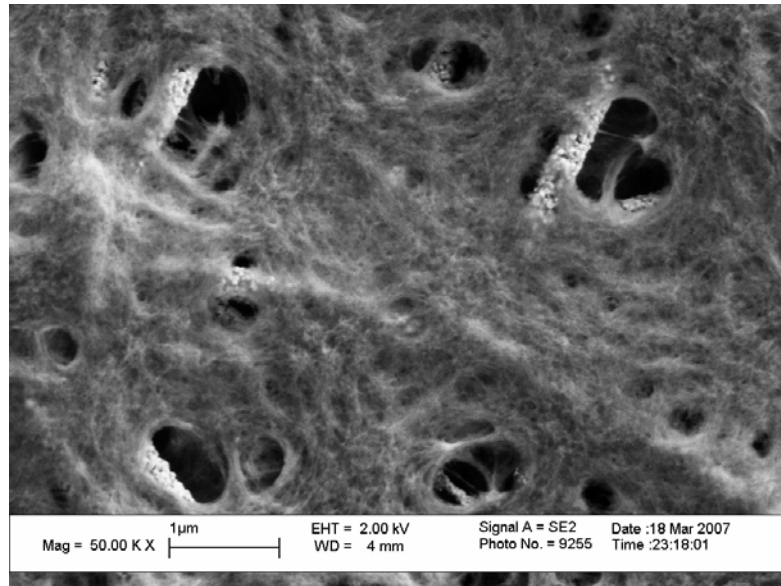


Figure 62 : A magnified image of Figure 61. Note on PVDF laying over and between the ZnO fibers.

4.3.2 ZnO / PVDF Nanopowder Composite

The SEM image in Figure 63 below belongs to the ZnO / PVDF nanopowder composite.

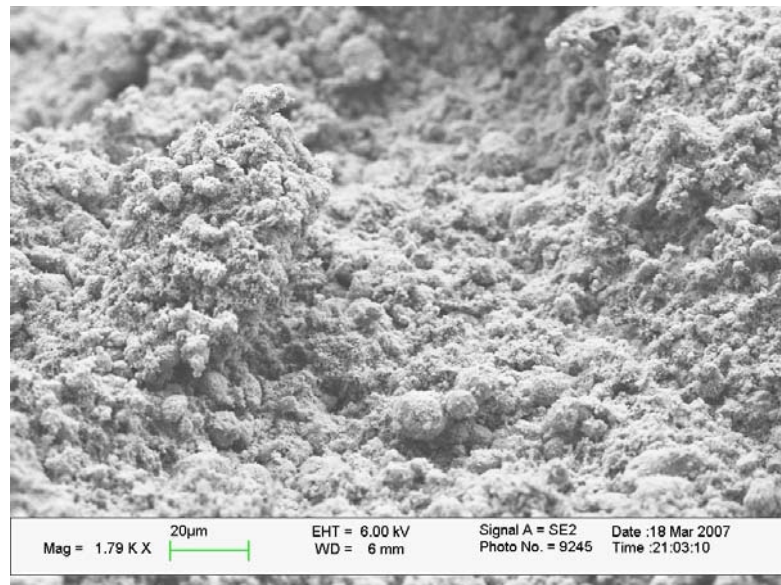


Figure 63 : SEM image of nanopowder-based composite.

4.3.3 Electromechanical Characterization

Electromechanical ability is measured on the composite pellets as in Figure 64. The nature of the response for all composites is concluded to be piezoelectric because as

the polarity of the excitation changed, response curve also switched sign. In addition, the method applied in PVDF electrospun fiber mats in section 3.3 is also applied.

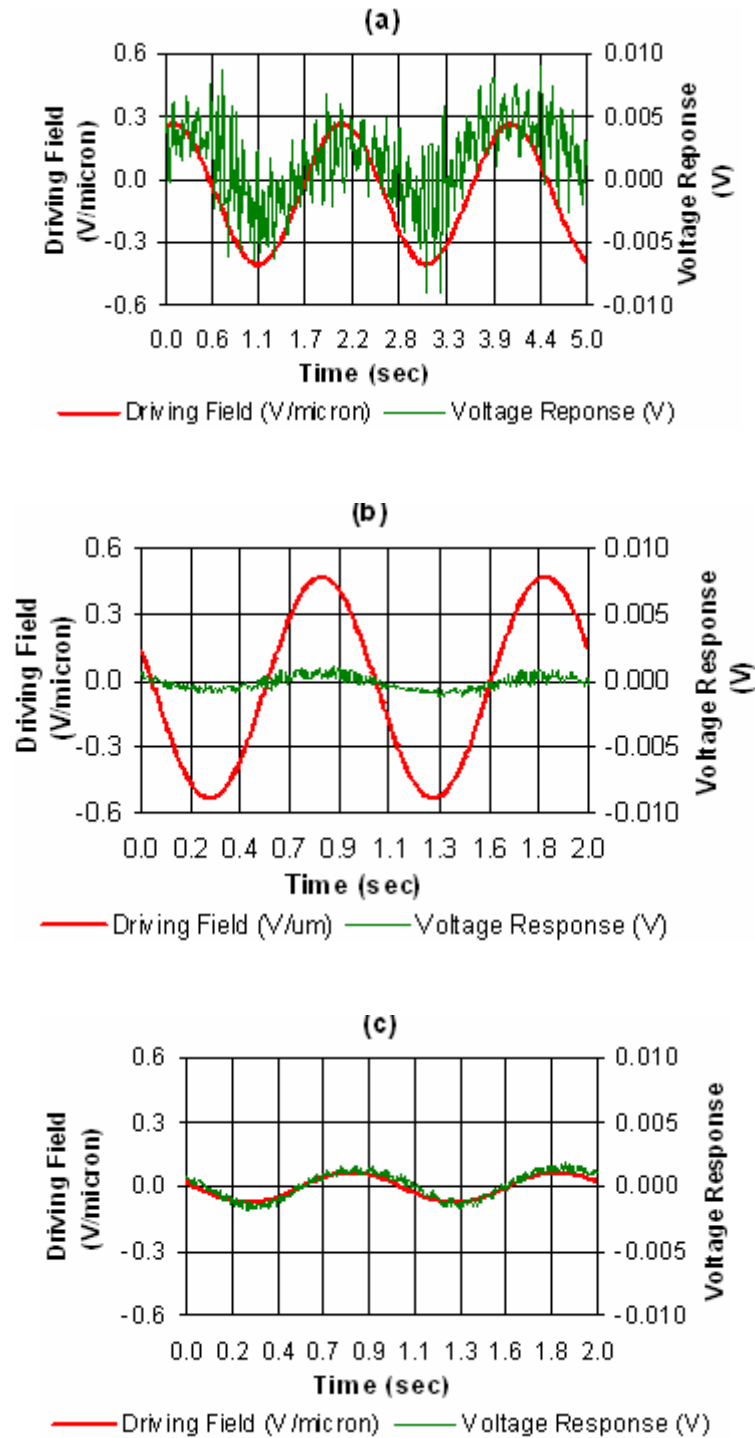


Figure 64 : Electromechanical response of PVDF/ZnO composite pellets: a) PVDF coated ZnO fibrous mat excited with 10V, 0.5Hz, b) PVDF coated ZnO fibrous mat laminated with PVDF excited with 50V, 1Hz, and c) PVDF and ZnO nanopowder-based composite excited with 50V, 1Hz sinusoidal.

5. SUGGESTIONS FOR FUTURE WORK

Based on the experimental experience some suggestions shall be given on the electromechanical measurements in order to reduce the workload and get more accurate results.

- For the electromechanical measurements a laser displacement sensor may be used instead of a photonic sensor because it may be less dependent on the surface morphology of the target. Thus, the same result accuracy may be obtained with less time spent to calibrate the sensor and get noise-free results during the measurements.
- As stated in Chapter 4, for the in-plane strain measurements, the reason for building a tube-like specimen from PVDF electrospun mats is to increase the working area at the edge of the mat, since it is not big enough for the photons to be reflected and sensed. A solution for this may be to use a fiber-optic edge position sensing system designed to measure the dynamic position of thin objects, which MTI Instruments Inc. also serves. This system may also enable one to measure the in-plane strain of ZnO because it does not allow to be bent, due to its brittleness.

As this thesis is one of the steps to reach the final goal, which is to utilize from electrospun PVDF as a piezoelectric actuator or sensor, future studies that should be done can be stated as follows.

Electrospinning

Up to present, a fixed collector has been used in electrospinning, which resulted in mats of nanofibers. Since these nanofibers were randomly aligned on the collector, macroscopically, the mats could be treated as isotropic in terms of their stress-strain

relationships (i.e. they have the same Young's and Shear Modulus in every direction). Thus, applying a certain stress in any direction would yield in the same strain response.

By using a rotating disc collector rather than a fixed one, the fibers can be aligned along the direction of rotation, so the film's yield strength will be enhanced in that direction. As a result, an increase in the films' sensor capability will be made because more external stress can be applied before reaching its yield strength; thus creating an increased amount of surface charge.

Using Additives

In a recent publication [17] the PVDF electrospinning solution is mixed with a salt, tetrabutylammonium chloride (TBAC), which claims a relative increase in the β -phase of the electrospun PVDF mats. As in that study, using TBAC as well as other additives should be on the agenda of the work, since if they may be effective, this may eliminate the necessity of poling to enhance the β -phase.

Poling

Since it is found that unpoled electrospun PVDF mats were not piezoelectric, they should be poled and electromechanical measurements should be made to search for their piezoelectricity.

In case it is determined that no piezoelectricity will ever exist without poling, the electrospinning should directly be performed on a potential device, for example a small wing skin to be used for morphing applications, and after, *corona poling* should be applied so as not to touch the coated wing skeleton during the process.

Using PZT rather than ZnO

So far in the experiments, electrospun ZnO has been rather than Lead Zirconate Titanate (PZT). ZnO is however very hard to work and has a very low piezoelectric strain coefficient compared to PZT. Thus, ZnO may be replaced with PZT in its fiber form, again to be produced by electrospinning.

6. CONCLUDING REMARKS

In this thesis, the first purpose was to reveal the electroactive characteristics of electrospun PVDF fibrous mats produced at specific electrospinning parameters to find out whether it is sufficient to use them as piezoelectric materials directly after their production. To the author's knowledge, electric field-strain relationship and nature of electroactivity of PVDF fiber mats were not directly measured and reported in the literature. Here, measurements revealed that under the current electrospinning process parameters no piezoelectricity existed, but the mats rather behaved as linear dielectrics. Based on these results, to characterize them for the sake of future studies, their transition from electrostrictive to linear dielectric behaviour was also recorded.

The second purpose was to produce ZnO/PVDF electroactive composites in case that PVDF directly be produced as a piezoelectric in future studies, as well as to utilize from ZnO, which -as a brittle piezoelectric material- does not require poling. In the first process, a ZnO fibrous mat is dipped into a PVDF solution to handle with the brittle ceramic fibers. In the second, a highly loaded ZnO/PVDF nanopowder composite is manufactured. As a result, relatively flexible piezoelectric composite pellets were obtained and electroactivity measurements revealed piezoelectric behaviour of the composites.

7. BIBLIOGRAPHY

1. Bharti, V. and R. Nath, *Piezo-, pyro-and ferroelectric properties of simultaneously stretched and corona poled extruded poly(vinyl chloride) films*. J. Phys. D: Appl. Phys, 2001. **34**: p. 667–672.
2. Sarkisov, S.S., et al., *Light-driven actuators based on polymer films*. Optical Engineering, 2006. **45**: p. 034302.
3. Fu, Y., et al., *Design, fabrication and testing of piezoelectric polymer PVDF microactuators*. Smart Materials and Structures, 2006. **15**(1): p. 141.
4. Pawlowski, K.J., et al., *Electrospinning of a micro-air vehicle wing skin*. Polymer, 2003. **44**(4): p. 1309-1314.
5. Chaudhuri, A.S. and A. Mukherjee, *Active control of piezolaminated columns-exact solutions and experimental validation*. Smart Materials and Structures, 2005. **14**(4): p. 475-482.
6. Dargaville, T.R., M. Celina, and P.M. Chaplya, *Evaluation of piezoelectric PVDF polymers for use in space environments. Part I: Temperature limitations*. J. Appl Polym Sci: Part B: Polymer Physics, 2005.
7. Gopal, R., et al., *Electrospun nanofibrous filtration membrane*. Journal of Membrane Science, 2006. **281**(1-2): p. 581-586.
8. Gu, H., Y. Zhao, and M.L. Wang, *A wireless smart PVDF sensor for structural health monitoring*. Structural Control and Health Monitoring, 2005. **12**(3): p. 329-343.
9. Dargahi, J., M. Parameswaran, and S. Payandeh, *A micromachined piezoelectric tactile sensor for an endoscopic grasper-theory, fabrication and experiments*. Microelectromechanical Systems, Journal of, 2000. **9**(3): p. 329-335.
10. Huang, A.L., J. Tai, and C.M. Ho, *Microsensors and actuators for macrofluidic control*. Sensors Journal, IEEE, 2004. **4**(4): p. 494-502.

11. Kwon, O.Y. and Y. Dzenis, *Embedded PVDF film sensor for in-situ monitoring of structural integrity of laminated composites*. Key Engineering Materials, 2004. **270**: p. 1929-1934.
12. Zhao, Z., et al., *Preparation and properties of electrospun poly (vinylidene fluoride) membranes*. Journal of Applied Polymer Science, 2005. **97**(2): p. 466-474.
13. Manesh, K.M., et al., *Electrospun poly (vinylidene fluoride)/poly (aminophenylboronic acid) composite nanofibrous membrane as a novel glucose sensor*. Analytical Biochemistry, 2007. **360**(2): p. 189-195.
14. Choi, S.S., et al., *Electrospun PVDF nanofiber web as polymer electrolyte or separator*. Electrochimica Acta, 2004. **50**(2): p. 339-343.
15. Kim, J.R., et al., *Electrospun PVdF-based fibrous polymer electrolytes for lithium ion polymer batteries*. Electrochimica Acta, 2004. **50**(1): p. 69-75.
16. Lee, K.P., et al., *Influence of finely dispersed carbon nanotubes on the performance characteristics of polymer electrolytes for lithium batteries*. Nanotechnology, IEEE Transactions on, 2007. **6**(3): p. 362-367.
17. Yee, W.A., et al., *Morphology, polymorphism behaviour and molecular orientation of electrospun poly(vinylidene fluoride) fibers*. Polymer, 2007. **48**(2): p. 512-521.
18. Harrison, J.S., et al., *Electrospun electroactive polymers*. 2006: U.S.A.
19. Yordem, O.S., *Piezoelectric ultrafine polymer and ceramic fibers by electrospinning: Process development and characterization*. 2006, Sabanci University.
20. Roy, S. and S. Basu, *Improved zinc oxide film for gas sensor applications*. Bull. Mater. Sci, 2002. **25**(6): p. 513-515.
21. Chronakis, I.S., *Novel nanocomposites and nanoceramics based on polymer nanofibers using electrospinning process—A review*. Journal of Materials Processing Tech., 2005. **167**(2-3): p. 283-293.
22. Sigmund, W., et al., *Processing and structure relationships in electrospinning of ceramic fibre systems*. Journal of the American Ceramic Society, 2006. **89**(2): p. 395-407.
23. Wang, Y., et al., *Synthesis and characterisation of ultra-fine tin oxide fibres using electrospinning*. Journal of the American Ceramic Society, 2005. **88**(8): p. 2059-2063.
24. Wu, H. and W. Pan, *Preparation of zinc oxide nanofibres by electrospinning*. Journal of the American Ceramic Society, 2006. **89**(2): p. 699-701.

25. Yang, X., et al., *Preparation and characterization of ZnO nanofibers by using electrospun PVA/zinc acetate composite fiber as precursor*. Inorg. Chem. Commun, 2004. **7**(2): p. 176–8.
26. Viswanathamurthi, P., et al., *The photoluminescence properties of zinc oxide nanofibres prepared by electrospinning*. Nanotechnology, 2004. **15**(3): p. 320-323.
27. Wu, H., et al., *Oriented nanofibers by a newly modified electrospinning method*. Journal of the American Ceramic Society, 2007. **90**(2): p. 632-634.
28. Hong, Y., et al., *In situ growth of ZnO nanocrystals from solid electrospun nanofiber matrixes*. Langmuir, 2006. **22**(17): p. 7331-7334.
29. Cui, C., et al., *Improved piezoelectric 0-3 ceramic particle/polymer composites*. Ferroelectrics, 1996. ISAF'96., Proceedings of the Tenth IEEE International Symposium on Applications of, 1996. **2**.
30. Lee, Y.S., S.J. Elliott, and P. Gardonio, *Matched piezoelectric double sensor/actuator pairs for beam motion control*. Smart Materials and Structures, 2003. **12**(4): p. 541-548.
31. Kim, K.Y., et al., *Performance evaluation of lightweight piezo-composite actuators*. Sensors and Actuators A: Physical, 2005. **120**(1): p. 123-129.
32. Brown, L.F., *Design considerations for piezoelectric polymer ultrasound transducers*. Ultrasonics, Ferroelectrics and Frequency Control, IEEE Transactions on, 2000. **47**(6): p. 1377-1396.
33. Brown, L.F. and J.L. Mason, *Disposable PVDF ultrasonic transducers for nondestructive testing applications*. Ultrasonics, Ferroelectrics and Frequency Control, IEEE Transactions on, 1996. **43**(4): p. 560-568.
34. Omote, K. and H. Ohigashi, *Properties of transverse ultrasonic transducers of ferroelectric polymers working in thickness shear modes*. Ultrasonics, Ferroelectrics and Frequency Control, IEEE Transactions on, 1996. **43**(2): p. 312-318.
35. Poizat, C. and M. Sester, *Effective properties of composites with embedded piezoelectric fibres*. Computational Materials Science, 1999. **16**(1): p. 89-97.
36. Stiffler, R. and E.G. Henneke, *The application of polyvinylidene fluoride as an acoustic emission transducer for fibrous composite materials*. Materials Evaluation, 1983. **41**: p. 956-960.
37. Su, J., et al., *An electroactive polymer-ceramic hybrid actuation system for enhanced electromechanical performance*. Applied Physics Letters, 2004. **85**: p. 1045.

38. Dzenis, Y., et al., *Manufacturing of novel continuous nanocrystalline ceramic nanofibers with superior mechanical properties*. NSF Nanoscale Science and Engineering Grantees Conference, Arlington, VA, Dec, 2003: p. 16–18.
39. Stroyan, J.J., *Processing and Characterization of PVDF, PVDF-TrFE, and PVDF-TrFE-PZT Composites*. 2004, Washington State University.
40. Kowbel, W., et al., *PZT/PVDF flexible composites for actuator and sensor applications*. Smart materials and technologies, 1998: p. 106-114.
41. Seoul, C., Y.T. Kim, and C.K. Baek, *Electrospinning of poly (vinylidene fluoride)/dimethylformamide solutions with carbon nanotubes*. Journal of Polymer Science Part B Polymer Physics, 2003. **41**(13): p. 1572-1577.
42. Chiang, Y., D.P. Birnie, and W.D. Kingery, *Physical ceramics*. 1997: J. Wiley.
43. Hummerl, R.E., *Electronic properties of materials*. 2001: Springer.
44. Ukraine, O., *Corona poling of ferroelectric and nonlinear optical polymers*. Moldovian Journal of the Physical Sciences, 2002.
45. Bharti, V., T. Kaura, and R. Nath, *Ferroelectric hysteresis in simultaneously stretched and corona-poled PVDF films*. Dielectrics and Electrical Insulation, IEEE Transactions on [see also Electrical Insulation, IEEE Transactions on], 1997. **4**(6): p. 738-741.
46. Kaura, T., R. Nath, and M.M. Perlman, *Simultaneous stretching and corona poling of PVDF films*. Journal of Physics D. Applied Physics, 1991. **24**: p. 1848-52.
47. Bar-Cohen, Y., et al., *Electroactive Polymers and Rapid Prototyping as held at the 2001 MRS Fall Meeting*. 2001.
48. Formhals, A., *Process and apparatus for preparing artificial threads*. 1934, Google Patents.
49. Doshi, J. and D.H. Reneker, *Electrospinning process and applications of electrospun fibers*. Industry Applications Society Annual Meeting, 1993., Conference Record of the 1993 IEEE, 1993: p. 1698-1703.
50. Deitzel, J.M., et al., *The effect of processing variables on the morphology of electrospun nanofibers and textiles*. Polymer, 2001. **42**(1): p. 261-272.
51. Demir, M.M., et al., *Electrospinning of polyurethane fibers*. Polymer, 2002. **43**(11): p. 3303-3309.

52. Mo, X.M., *Electrospun P(LLA-CL) nanofiber: a biomimetic extracellular matrix for smooth muscle cell and endothelial cell proliferation*. *Biomaterials*, 2004. **25**(10): p. 1883-1890.
53. Larrondo, L. and R. St John Manley, *Electrostatic fiber spinning from polymer melts. I. Experimental observations on fiber formation and properties*. *Journal of Polymer Science Polymer Physics Edition*, 1981. **19**(6): p. 909-920.
54. Sukigara, S., et al., *Regeneration of Bombyx mori silk by electrospinning. Part 2. Process optimization and empirical modeling using response surface methodology*. *Polymer*, 2004. **45**(11): p. 3701-3708.
55. Yordem, O.S., M. Papila, and Y.Z. Menciloglu. *Prediction of electrospinning parameters for targeted nanofiber diameter*. in *Nanocomposites*. 2005.
56. Dawley, J.T., et al., *Piezoelectric characterization of bulk and thin film ferroelectric materials using fiber optics*. MTI Instruments Inc., Application Note.
57. *Ltd. E. EMITECH K350 Attachment (Sputter Coating/Glow Discharge) Instruction Manual*. 2000.